

Coverage in Multi-Antenna Two-Tier Networks

Vikram Chandrasekhar, Marios Kountouris and Jeffrey G. Andrews

Abstract

In two-tier networks – comprising a conventional cellular network overlaid with shorter range hotspots (e.g. femtocells, distributed antennas, or wired relays) – with universal frequency reuse, the near-far effect from cross-tier interference creates dead spots where reliable coverage cannot be guaranteed to users in either tier. Equipping the macrocell and femtocells with multiple antennas enhances robustness against the near-far problem. This work derives the maximum number of simultaneously transmitting multiple antenna femtocells meeting a per-tier outage probability constraint. Coverage dead zones are presented wherein cross-tier interference bottlenecks cellular and hotspot coverage. Two operating regimes are shown namely 1) a cellular-limited regime in which femtocell users experience unacceptable cross-tier interference and 2) a hotspot-limited regime wherein both femtocell users and cellular users are limited by hotspot interference. Our analysis accounts for the per-tier transmit powers, the number of transmit antennas (single antenna transmission being a special case) and terrestrial propagation such as the Rayleigh fading and the path loss exponents. Single-user (SU) multiple antenna transmission at each tier is shown to provide significantly superior coverage and spatial reuse relative to multiuser (MU) transmission. We propose a decentralized carrier-sensing approach to regulate femtocell transmission powers based on their location. Considering a worst-case cell-edge location, simulations using typical path loss scenarios show that our interference management strategy provides reliable cellular coverage with about 60 femtocells per cellsite.

I. INTRODUCTION

Wireless operators are in the process of augmenting the macrocell network with supplemental infrastructure such as microcells, distributed antennas and relays. An alternative with lower upfront costs is to improve indoor coverage and capacity using the concept of *end-consumer* installed femtocells or home base stations [1]. A femtocell is a low power, short range (10 – 50 meters) wireless data access point (AP) that provides in-building coverage to home users and transports the user traffic over internet based backhaul such as cable modem. Because of the proximity of users to their APs, femtocells provide higher spatial reuse of spectrum and cause less interference to other users. The spatial reuse (in

This research has been supported by Texas Instruments Inc. V. Chandrasekhar, M. Kountouris and J. G. Andrews are with the Wireless Networking and Communications Group, Dept. of Electrical and Computer Engineering at the University of Texas at Austin. (email: cvikram@mail.utexas.edu, (mkountouris, jandrews)@ece.utexas.edu), Date: April 12, 2019.

b/s/Hz/m²) is readily expressible by the area spectral efficiency (ASE) [2] which is a measure of the total obtainable network throughput per unit Hz per unit area. Previous studies [1] have shown a nearly 25x improvement in overall spatial reuse when moving from a macrocell-only network to a two-tier underlay with 50 femtocells per cellsite.

In addition to improved spatial reuse, cellular operators desire to operate both cellular and indoor femtocell users in the same bandwidth (universal frequency reuse), as is assumed in this paper, for cost effectiveness and flexible deployment [3]. With shared spectrum, practical challenges stem from the absence of coordination across tiers [1], [4] due to scalability issues. Because femtocells are consumer deployed in their self-interest and because of reasons of security and limited backhaul capacity, these femtocells will potentially offer privileged coverage only to licensed, subscribed indoor users. This paper assumes *Closed Access* (CA), which means only licensed home users within radio range can communicate with their own femtocell. The drawback of such a co-channel closed access deployment of femtocells is that cross-tier interference (Fig. 1) becomes the capacity-limiting factor. Commercial femtocell offerings (such as Verizon’s “home network expander”) provide both public access (by default) and a closed access operation which are user configurable. Our results provide a networkwide performance benchmark in a closed access setting.

A. Problem Definition

The motivation behind this paper is to understand how exploiting the available degrees of freedom through multiple antenna transmission influences coverage and spatial reuse in a two-tier network with universal frequency reuse. We consider both single-user (SU) multiple antenna transmission and multiuser (MU) multiple antenna transmission (Fig. 2) employed by the macrocell basestation (BS) and femtocell APs. Array gain resulting from SU transmission provides robustness against cross-tier interference. Multiuser transmission, on the other hand, increases the number of simultaneous transmissions at the expense of reduced signal strength per user terminal and potential inter-user interference.

Given a multiple antenna transmission strategy (SU or MU), let λ_f denote the maximum density (in femtocells per square meter) of simultaneously transmitting femtocells – denoted as the *maximum femtocell contention density* – that guarantees a certain minimum per-tier Quality of Service (QoS) requirement. Given a certain minimum per-tier target Signal-to-Interference Ratio (SIR) equaling β , the QoS requirement stipulates that the instantaneous SIR at each user should exceed β with a probability of at least $1 - \epsilon$, where ϵ is a design parameter. Since the signal power for a cellular user decays as $D^{-\alpha_c}$ (D being the distance from the macrocell BS and α_c is the outdoor path loss exponent), satisfying its

QoS requirement requires λ_f to be a monotonically decreasing function of D . Conversely, satisfying the QoS requirement for a femtocell user at D necessitates λ_f to be monotonically decreasing as $D \rightarrow 0$.

This paper characterizes near-far effects by defining two quantities of interest namely the *No-Coverage Femtocell Radius* and the *Cellular Coverage Radius*. The no-coverage femtocell radius D_f determines the minimum SIR feasible femtocell distance from the macrocell. Any femtocell user within $D < D_f$ meters from the macrocell experiences an outage probability greater than ϵ due to excessive cellular interference. This suggests that any user at $D < D_f$ should communicate with the macrocell because of its potentially higher cellular SIR. The cellular coverage radius D_c denotes the maximum SIR feasible distance from the macrocell up to which a cellular user can satisfy its outage probability constraint in the presence of hotspot interference. Since there is no coordination between tiers for managing interference, providing greater spatial reuse using femtocells trades off the coverage radiuses and vice-versa. Because the cellular network serves as the primary network to mobile outdoor users, it is desirable to maximize D_c in the presence of hotspot interference.

Assuming that each tier employs either transmit beamforming (BF) [for SU transmission] or linear zero-forcing precoding [for MU transmission] with transmission powers P_c and P_f in each resource (eg. frequency sub-band), this work poses the following questions:

- What is the maximum femtocell contention density λ_f as a function of the location D with respect to (w.r.t) the macrocell, the ratio P_c/P_f , the transmission strategy (SU vs. MU transmission), the number of transmit antennas per macrocell and femtocell AP, the target per-tier SIR β , the maximum outage probability ϵ and the path loss exponents?
- Given an average of N_f transmitting femtocells per cell-site, how much cellular coverage can the macrocell provide to its users?
- How does the no-coverage femtocell radius vary with SU and MU femtocell transmission strategies?
- How should femtocells adapt their transmission power as a function of their location w.r.t the macrocell for ensuring that nearby cellular users satisfy their QoS requirements?

B. Related Work

Prior research in tiered networks have mainly considered an operator planned underlay of a macrocell with single/multiple microcells [5]–[7]. A microcell has a much larger radio range (100-500 m) than a femtocell, and generally implies centralized deployment, i.e. by the service-provider. This allows the operator to either load balance users [8], [9] or preferentially assign high data rate cellular users to the microcell [10], [11] because of its inherently larger capacity. In contrast, femtocells are consumer

installed and the traffic requirements at femtocells are user determined without any operator influence. Consequently, decentralized strategies for interference management may be preferred [1], [12]–[14].

The subject of this work is related to Huang *et al.* [15] which derives per-tier transmission capacities with spectrum underlay and spectrum overlay. In contrast to their work which assumes relay-assisted cell-edge users, our work proposes to improve coverage by regulating femtocell transmit powers. Hunter *et al.* [16] have derived transmission capacities in an *ad hoc* network with spatial diversity. Our work has extended this analysis to a cellular-underlaid *ad hoc* network. To the best of our knowledge, there is little related work addressing diversity performance in tiered networks (e.g [17] which proposes tilted antenna arrays to reduce cross-tier interference).

Finally, related works on cognitive radios (CR) include (but not restricted to) 1) analyzing sensing-throughput tradeoffs [18] for computing optimal sensing time by CR users and 2) limit transmit powers of CR users [19]–[22]. The differentiating aspect of our work is a decentralized femtocell transmit power selection scheme which ensures a per-tier outage probability below a desired threshold.

C. Contributions

Given T_c antennas at the macrocell and T_f antennas at each femtocell, per-tier transmission powers equaling P_c at the macrocell and P_f at each femtocell, and path loss exponents given as α_c (from outdoor cellular transmission) and α_{fo} (from femtocell transmission to outdoor users and neighboring femtocells) respectively, our work provides the following contributions.

Coverage. We derive coverage zones wherein cross-tier interference prevents users in each tier from satisfying their QoS requirements. Single-user macrocell transmission is shown to increase the cellular coverage radius by a factor T_c^{2/α_c} relative to MU transmission. Single-user femtocell transmission is shown to decrease the no-coverage femtocell radius D_f by a factor of $(T_f/\epsilon^{1-1/T_f})^{1/\alpha_c}$ relative to MU femtocell transmission. This suggests that the array gain provided by SU transmission results in superior coverage in either tier. Moreover, a femtocell located just a few meters outside the no-coverage zone can tolerate interference from greater than 100 hotspots per cellsite. This suggests that femtocell performance is regulated by cellular interference and hotspot interference is negligible in comparison.

Hotspot Contention Density. We derive the maximum femtocell contention density $\lambda_f(D)$ at distance D from the macrocell. Two distinct operating regimes are shown namely a 1) Cellular-limited regime, wherein femtocell users are primarily affected by cellular interference and 2) Hotspot-limited regime wherein both cellular and hotspot users are affected by hotspot interference. Regime 1 determines the coverage provided to hotspot users, while Regime 2 determines the maximum hotspot contention density that satisfies a maximum per-tier outage probability constraint. In Regime 2, SU macrocell

transmission is shown to provide a factor of $\Gamma(1 - 2/\alpha_{fo})T_c^{4/\alpha_{fo}}$ increase in the maximum femtocell contention density relative to MU transmission. Femtocells maximize their area spectral efficiency by choosing their transmission strategy depending on α_{fo} , with SU transmission being desirable with considerable hotspot interference ($\alpha_{fo} < 4$). This suggests that SU transmission in either tier provides higher spatial reuse in realistic path loss scenarios.

Power control. We propose a carrier-sensing approach in which a femtocell chooses its transmission power P_f in order to minimize hotspot interference and ensure uniform cellular coverage. We derive lower and upper bounds for P_f depending on the femtocell location, the number of macrocell and femtocell antennas and the path loss exponents. We demonstrate that our strategy enables uniform cellular coverage with up to 60 femtocells per cell site (with typical cellular parameters).

II. SYSTEM MODEL

Assume a central macrocell B_0 using T_c antennas to service a geographical region \mathcal{C} , assumed as a circular disc with radius R_c and area $|\mathcal{C}| = \pi R_c^2$. Each femtocell is equipped with T_f antennas. Both cellular users and femtocell users are assumed to be equipped with single-antenna receivers. In a given time/frequency slot, each macrocell [resp. femtocell] employs its T_c [resp. T_f] antennas for serving $1 \leq U_c \leq T_c$ cellular [resp. $1 \leq U_f \leq T_f$ indoor] users.

This paper employs a stochastic geometry framework for modeling the random spatial distribution of the underlying femtocells. Hotspot locations are likely to vary from one cell site to another, and be opportunistic rather than planned, so an analysis that embraces instead of neglecting randomness should provide more accurate results and more plausible insights. The randomly located femtocells are assumed to be distributed according to a Spatial Poisson Point Process (SPPP) Π_f (see [23], [24] for background, prior works include [25]–[27]). Provided Π_f is a homogeneous SPPP (or the intensity λ_f in femtocells per square meter stays constant over \mathcal{C}), the average number of actively transmitting femtocells is readily obtained as $N_f = \lambda_f |\mathcal{C}|$ femtocells per cellsite. Because of near-far effects inherent to a two-tier network, the maximum hotspot intensity varies with the location D in the cell-site.

A. Terrestrial Path Loss Model

The signal decay encountered using terrestrial propagation is represented using a distance based path loss model. Temporal amplitude variations of the complex vector downlink channel are modeled as frequency-flat Rayleigh fading – e.g. each frequency sub-band in frequency division multiple access (FDMA) transmission – with individual complex entries distributed as $\mathcal{CN}(0, 1)$. For analytical simplicity, this work does not consider random lognormal shadow fading. Instead, we shall assume a

fixed partition loss, based on Qualcomm's home BS propagation model [28], which accounts for wall losses encountered during outdoor-to-indoor and indoor-to-indoor propagation. Shown below, we use the IMT-2000 channel model [29] for modeling indoor and outdoor path losses.

Macrocell to Cellular Users. The decibel path loss between B_0 and cellular user 0 is modeled as $PL_{c,\text{dB}} = A_{c,\text{dB}} + 10\alpha_c \log_{10} D$ where α_c is the outdoor path loss exponent, $A_{c,\text{dB}} = 30 \log_{10} f_c - 71$ represents the fixed decibel loss during outdoor propagation, f_c is the carrier frequency in MHz and D is the distance between B_0 and its user.¹

Macrocell to Femtocell Users. We model each femtocell as a point object, hence all indoor users served by a given femtocell experience an identical average cellular interference. This decibel path loss is given as $PL_{f,c,\text{dB}} = A_{f,c,\text{dB}} + 10\alpha_c \log_{10}(D)$ where $A_{f,c,\text{dB}} = 30 \log_{10} f_c - 71 + W_{\text{dB}}$ designates the fixed decibel path loss, D is the distance between B_0 and the femtocell and W_{dB} equals the decibel wall partition loss during outdoor-to-indoor wireless propagation.

Femtocell to Subscribed Home Users. The decibel path loss between a femtocell to its licensed, subscribed indoor users is modeled as $PL_{f,i,\text{dB}} = A_{f,i,\text{dB}} + 10\alpha_{fi} \log_{10}(R_f)$ where $A_{f,i,\text{dB}} = 37$ dB models the fixed propagation loss in decibels between the femtocell to its desired user, α_{fi} represents the indoor path loss exponent and R_f denotes the radio range of the femtocell. For analytical simplicity and modeling the worst-case scenario, we assume that indoor users are located on the edge of their respective femtocells.

Femtocell to Outdoor Cellular Users. Given a transmitting femtocell, any cellular user located at distance D will experience cross-tier interference with decibel path loss modeled as $PL_{c,f,\text{dB}} = A_{c,f,\text{dB}} + 10\alpha_{fo} \log_{10}(D)$. Here, the fixed decibel path loss is designated by $A_{c,f,\text{dB}} = W_{\text{dB}} + 37$, while α_{fo} denotes the path loss exponent during indoor-to-outdoor wireless propagation.

Femtocell to Neighboring Femtocells. The decibel path loss of the hotspot interference caused by a transmitting femtocell at another femtocell is given as $PL_{f,f,\text{dB}} = A_{f,f,\text{dB}} + 10\alpha_{fo} \log_{10}(D)$ where $A_{c,f} = 2W_{\text{dB}} + 37$ denotes the fixed decibel path loss (the factor of 2 models the double wall partition loss during indoor to indoor propagation) and D is the distance between the two femtocells.

III. PER-TIER SIGNAL-TO-INTERFERENCE RATIOS

Assume that the macrocell B_0 serves $1 \leq U_c \leq T_c$ users. Define $\mathbf{h}_j \in \mathbb{C}^{T_c \times 1}$ as the channel from B_0 to cellular user $j \in \{0, 1, \dots, U_c - 1\}$ with its entries distributed as $h_{k,j} \sim \mathcal{CN}(0, 1)$. The direction of

¹Strictly speaking, the IMT-2000 pedestrian test model adopts a fixed path loss exponent $\alpha_c = 4$ (with path loss $PL_{\text{dB}} = 30 \log_{10} f_c + 40 \log_{10}(D) - 71$). To keep the analysis general, this paper parameterizes the outdoor path loss exponent.

each vector channel is represented as $\tilde{\mathbf{h}}_j \triangleq \frac{\mathbf{h}_j}{\|\mathbf{h}_j\|}$. Designate $\tilde{\mathbf{H}} = [\tilde{\mathbf{h}}_0, \tilde{\mathbf{h}}_1, \dots, \tilde{\mathbf{h}}_{U_c-1}]^\dagger \in \mathbb{C}^{U_c \times T_c}$ as the concatenated matrix of channel directions, where the symbol \dagger denotes conjugate transpose.

AS 1: Perfect channel state information (CSI) is assumed at the central macrocell [resp. femtocells] regarding the channels to their own users.

Although we acknowledge that imperfect channel estimation plays a potentially significant role, we defer its analysis for subsequent research and instead employ AS1 for analytical tractability.

AS 2: Cochannel Interference from neighboring cellular transmissions is negligibly small.

We justify AS2 as reasonable considering that contemporary wireless standards such as the 802.16 WiMAX perform fractional frequency reuse [30] to limit cell-edge interference.

This work assumes linear zero-forcing (ZF) precoding transmission because it has low complexity, but achieves the same multiplexing gain as higher complexity schemes such as dirty-paper coding. With ZF precoding transmission, B_0 chooses its precoding matrix $\mathbf{V} \in \mathbb{C}^{T_c \times U_c}$ as the normalized columns of the pseudoinverse $\tilde{\mathbf{H}}^\dagger (\tilde{\mathbf{H}} \tilde{\mathbf{H}}^\dagger)^{-1} \in \mathbb{C}^{T_c \times U_c}$. Similarly, each femtocell $F_j \in \Pi_F$ serves $1 \leq U_f \leq T_f$ users with the channel directions between F_j to its individual users represented as $\mathbf{G}_j^\dagger = [\tilde{\mathbf{g}}_{0,j}, \tilde{\mathbf{g}}_{1,j}, \dots, \tilde{\mathbf{g}}_{U_f-1,j}]$ and the entries of $\tilde{\mathbf{g}}_{k,j}$ distributed as $\mathcal{CN}(0, 1)$. With ZF precoding, the precoding matrix $\mathbf{W}_j \in \mathbb{C}^{T_f \times U_f}$ equals the normalized columns of $\tilde{\mathbf{G}}^\dagger (\tilde{\mathbf{G}} \tilde{\mathbf{G}}^\dagger)^{-1} \in \mathbb{C}^{T_f \times U_f}$.

A. SIR Analysis at a Femtocell User

Consider a reference femtocell F_0 at distance D from the macrocell B_0 . During a given signaling interval, the received signal at femtocell user 0 at distance R_f w.r.t F_0 is given as

$$y_0 = \underbrace{\sqrt{A_{f,i}} R_f^{-\frac{\alpha_{f,i}}{2}} \mathbf{g}_0^\dagger \mathbf{W}_0 \mathbf{r}_0}_{\text{Desired Signal}} + \underbrace{\sqrt{A_{f,f}} \sum_{F_j \in \Pi_f \setminus F_0} |X_{0,j}|^{-\frac{\alpha_{f,o}}{2}} \mathbf{g}_{0,j}^\dagger \mathbf{W}_j \mathbf{r}_j}_{\text{Intra-tier Interference}} + \underbrace{\sqrt{A_{f,c}} D^{-\frac{\alpha_c}{2}} \mathbf{f}_0^\dagger \mathbf{V} \mathbf{s} + \mathbf{n}}_{\text{Cross-tier Interference}}$$

where the vectors $\mathbf{s} \in \mathbb{C}^{U_c \times 1}$ and $\mathbf{r}_j \in \mathbb{C}^{U_f \times 1}$ designate the transmit data symbols for users in B_0 and F_j , which satisfy $\mathbb{E}[\|\mathbf{s}\|^2] \leq P_c$ and $\mathbb{E}[\|\mathbf{r}_j\|^2] \leq P_f$ respectively (assuming equal power allocation) and \mathbf{n} represents background noise. The term $\mathbf{f}_0 \in \mathbb{C}^{T_c \times 1}$ [resp. $\mathbf{g}_{0,j}$] designates the downlink vector channel from the interfering macrocell BS B_0 [resp. interfering femtocell AP F_j] to user 0. Neglecting receiver noise for analytical simplicity, the received SIR for user 0 is given as

$$\text{SIR}_f(F_0, D) = \frac{\frac{P_f}{U_f} A_{f,i} R_f^{-\alpha_{f,i}} \|\mathbf{g}_0\|^2}{\frac{P_c}{U_c} A_{f,c} D^{-\alpha_c} \|\mathbf{f}_0^\dagger \mathbf{V}\|^2 + \frac{P_f}{U_f} A_{f,f} \sum_{F_j \in \Pi_f \setminus F_0} \|\mathbf{g}_{0,j}^\dagger \mathbf{W}_j\|^2 |X_{0,j}|^{-\alpha_{f,o}}} \quad (1)$$

For successfully decoding the message intended for user 0, $\text{SIR}_f(F_0, D)$ should be greater than equal to the minimum SIR target β . For clarity of exposition, we define

$$\mathcal{P}_f = \frac{P_c}{P_f} \frac{A_{f,c}}{A_{f,f}} D^{-\alpha_c}, \quad \mathcal{Q}_f = \frac{A_{f,f}}{A_{f,i}} R_f^{\alpha_{f,i}} U_f \quad (2)$$

User 0 can successfully decode its signal provided $\text{SIR}_f(F_0, D)$ is at least equal to its minimum SIR target β . Combining (1) and (2), the probability of successful reception is given as

$$\mathbb{P}[\text{SIR}_f(F_0, D) \geq \beta] = \mathbb{P}\left[\|\mathbf{g}_0\|^2 \geq \beta \mathcal{Q}_f \left(\frac{\mathcal{P}_f}{U_c} \|\mathbf{f}_0^\dagger \mathbf{V}\|^2 + \frac{1}{U_f} \sum_{j \in \Pi_F} \|\mathbf{g}_{0,j}^\dagger \mathbf{W}_j\|^2 |X_{0,j}|^{-\alpha_{f_0}} \right)\right] \quad (3)$$

$$\text{Let } \kappa = \frac{\mathcal{P}_f \mathcal{Q}_f \beta}{U_c} = \beta \frac{P_c/U_c}{P_f/U_f} \frac{A_{f,c}}{A_{f,i}} \frac{D^{-\alpha_c}}{R_f^{-\alpha_{f_i}}} \quad (4)$$

Note that $\kappa \geq 0$ and the expression $\frac{\kappa}{\kappa+1} \in [0, 1)$ characterizes the relative strength of cellular interference. As κ increases (or $\frac{\kappa}{\kappa+1} \rightarrow 1$), user 0 experiences progressively poor coverage due higher cellular interference. Conversely, as $\kappa \rightarrow 0$, $\text{SIR}_f(F_0, D)$ is limited by interference from neighboring femtocells.

For satisfying the femtocell QoS requirement, $\mathbb{P}[\text{SIR}_f(F_0, D) \geq \beta] \geq 1 - \epsilon$ in equation (3). The following theorem gives the *no-coverage femtocell radius* D_f as a function of ϵ , β , T_f , U_f and U_c .

Theorem 1: Any femtocell F_0 within $D < D_f$ meters of the macrocell B_0 cannot satisfy its QoS requirement ϵ , where D_f is given as

$$D_f = \left[\frac{K P_f/U_f}{\beta P_c/U_c} \left(\frac{\mathcal{I}^{-1}(\epsilon; T_f - U_f + 1, U_c)}{1 - \mathcal{I}^{-1}(\epsilon; T_f - U_f + 1, U_c)} \right) \right]^{-1/\alpha_c} \quad (5)$$

where $K = \frac{A_{f_i}}{A_{f,c}} R_f^{-\alpha_{f_i}}$ and $x \triangleq \mathcal{I}^{-1}(\epsilon; a, b)$ denotes the value of x for which the cdf of a Beta-distributed random variable X with parameters a and b [namely the regularized incomplete Beta function $\mathcal{I}_x(a, b) = \mathbb{P}(X \leq x)$] equals ϵ .

Proof: Refer to Appendix I. ■

Proposition 1: The inverse function $\mathcal{I}^{-1}(x; a, b)$ is monotonically increasing with a and monotonically decreasing with b for any $a, b \geq 0$.

Proof: Using $\Gamma(k) = (k-1)!$ to denote the Gamma function for any positive integer k , we use the following two expansions [31, Page 29] for $\mathcal{I}_x(a, b)$.

$$\mathcal{I}_x(a, b) \stackrel{(a)}{=} 1 - \sum_{i=1}^a \frac{\Gamma(b+i-1)}{\Gamma(b)\Gamma(i)} x^{i-1} (1-x)^b \stackrel{(b)}{=} \sum_{i=1}^b \frac{\Gamma(a+i-1)}{\Gamma(a)\Gamma(i)} x^a (1-x)^{i-1} \quad (6)$$

Relation (a) shows that $\mathcal{I}_x(a, b)$ monotonically decreases with a . The equivalent Relation (b) shows that $\mathcal{I}_x(a, b)$ is monotone increasing w.r.t b . Consequently, the inverse function $\mathcal{I}^{-1}(x; a, b)$ monotonically increases with a and monotonically decreases with b . ■

Remark 1: With SU femtocell transmission ($U_f = 1$), the no-coverage radius $D_{f,\text{SU}}$ is strictly smaller than the no-coverage radius $D_{f,\text{MU}}$ with MU transmission ($1 < U_f \leq T_f$). This follows by applying Proposition 1 to (5) in Theorem 1.

Corollary 1: With K as defined in Theorem 1 and $U_c = 1$, the reduction in the no-coverage radius using a SU transmission strategy at femtocells relative to MU transmission to $U_f = T_f$ users [resp. single antenna transmission] is given as

$$\begin{aligned} \frac{D_{f,\text{SU}}}{D_{f,\text{MU}}} &= \left[\left(\frac{1 - \epsilon^{1/T_f}}{\epsilon^{1/T_f}} \right) \frac{\epsilon}{1 - \epsilon} \frac{1}{T_f} \right]^{1/\alpha_c} \approx \left[\frac{\epsilon^{1-1/T_f}}{T_f} \right]^{1/\alpha_c} \\ \frac{D_{f,\text{SU}}}{D_{f,1 \text{ Antenna}}} &= \left[\left(\frac{1 - \epsilon^{1/T_f}}{\epsilon^{1/T_f}} \right) \frac{\epsilon}{1 - \epsilon} \right]^{1/\alpha_c} \approx \epsilon^{\frac{1}{\alpha_c}(1-1/T_f)} \end{aligned}$$

Proof: With SU femtocell transmission [resp. MU transmission to $U_f = T_f$ users] and $U_c = 1$ user, the incomplete beta function $\mathcal{I}_{\frac{\kappa}{\kappa+1}}(T_f - U_f + 1, U_c)$ simplifies as

$$\mathcal{I}_{\frac{\kappa_1}{\kappa_1+1}}(T_f, 1) = \left(\frac{\kappa_1}{\kappa_1 + 1} \right)^{T_f}, \quad \mathcal{I}_{\frac{\kappa_2}{\kappa_2+1}}(1, 1) = \left(\frac{\kappa_2}{\kappa_2 + 1} \right) \quad (7)$$

where $\kappa_1 = \frac{1}{K} \frac{P_c}{P_f} D_{f,\text{SU}}^{-\alpha_c}$ and $\kappa_2 = \frac{1}{K} \frac{P_c}{P_f/T_f} D_{f,\text{MU}}^{-\alpha_c}$ respectively. Therefore, the no-coverage distances in (5) are respectively given as

$$D_{f,\text{SU}} = \left[\frac{K}{\beta} \frac{P_f}{P_c} \left(\frac{\epsilon^{1/T_f}}{1 - \epsilon^{1/T_f}} \right) \right]^{-1/\alpha_c}, \quad D_{f,\text{MU}} = \left[\frac{K}{\beta} \frac{P_f/T_f}{P_c} \left(\frac{\epsilon}{1 - \epsilon} \right) \right]^{-1/\alpha_c} \quad (8)$$

Assuming small ϵ , SU femtocell transmission consequently reduces D_f by a factor of approximately $\left(\frac{T_f}{\epsilon^{1-1/T_f}} \right)^{1/\alpha_c}$ relative to MU transmission. A similar argument shows that SU transmission reduces D_f by a factor of approximately $\epsilon^{-\frac{1}{\alpha_c}(1-1/T_f)}$ relative to single antenna transmission. ■

Remark 2: For fixed T_f , U_f and U_c , the no-coverage femtocell radius D_f in (5) scales with the ratio of the per-tier transmission powers P_f/P_c as $(P_f/P_c)^{-1/\alpha_c}$. Decreasing D_f by a factor of k requires each femtocell to increase their transmit power by $10\alpha_c \log_{10} k$ decibels. This suggests that the graph of D_f versus P_f/P_c (see Fig. 3) is a straight line on a log-log scale with slope $-1/\alpha_c$.

Any femtocell located at a distance $D > D_f$ w.r.t the macrocell can tolerate interference from both the cellular transmissions as well as neighboring hotspot transmissions. Next, we derive the maximum obtainable spatial reuse from multiple antenna femtocells when they share spectrum with cellular transmissions. Mathematically, the *maximum femtocell contention density* at normalized distance D w.r.t the macrocell is expressed as

$$\lambda_f^*(D) = \arg \max \lambda_f, \quad \text{subject to } \mathbb{P}(\text{SIR}_f(F_0, D) \geq \beta) \geq 1 - \epsilon \quad (9)$$

The spatial throughput (in bits/s/Hz) in a local neighborhood with area $|\mathcal{A}|$ can be no greater than $\text{ASE}(D)|\mathcal{A}|$, where $\text{ASE}(D) \triangleq (1 - \epsilon) \log_2(1 + \beta) \lambda_f^*(D)$ represents the highest obtainable area spectral efficiency with outage constraint ϵ . The average spatial throughput (averaged over \mathcal{C}) is upper bounded by

$2\pi(1-\epsilon)\log_2(1+\beta)\int_0^{R_c} r\lambda_f^*(r)dr$. The following theorem derives the maximum femtocell contention density $\lambda_f^*(D)$ subject to a QoS requirement at each femtocell.

Theorem 2: In a two-tier network, the maximum femtocell contention density $\lambda_f^(D)$ at distance D from the macrocell B_0 , which satisfies (9) (in the small- ϵ regime) is given as*

$$\lambda_f^*(D) = \frac{1}{\mathcal{C}_f(\mathcal{Q}_f\beta)^{\delta_f}} \left[\frac{\epsilon - \mathcal{I}_{\frac{\kappa}{\kappa+1}}(T_f - U_f + 1, U_c)}{\frac{1}{\mathcal{K}_f} - \mathcal{I}_{\frac{\kappa}{\kappa+1}}(T_f - U_f + 1, U_c)} \right] \quad (10)$$

where $\delta_f = 2/\alpha_{f_0}$, \mathcal{Q}_f is given by (2), κ is given by (4), and

$$\mathcal{C}_f = \pi\delta_f U_f^{-\delta_f} \sum_{k=0}^{U_f-1} \binom{U_f}{k} B(k + \delta_f, U_f - k - \delta_f) \quad (11)$$

$$\mathcal{K}_f = \left[1 + \frac{1}{(1+\kappa)^{U_c}} \sum_{j=0}^{T_f-U_f-1} \left(\frac{\kappa}{\kappa+1} \right)^j \binom{U_c+j-1}{j} \sum_{l=1}^{T_f-U_f-j} \frac{1}{l!} \prod_{m=0}^{l-1} (m - \delta_f) \right]^{-1} \quad (12)$$

where $B(a, b) = \frac{\Gamma(a)\Gamma(b)}{\Gamma(a+b)}$ denotes the Beta function and $\mathcal{K}_f = 1$ whenever $U_f = T_f$.

Proof: Refer to Appendix II ■

Theorem 2 provides the maximum femtocell contention density at D considering both cross-tier cellular and hotspot interference from neighboring femtocells. Alternatively, given an average of λ_f transmitting femtocells per square meter, (10) can be inverted (numerically) to obtain the minimum D which guarantees that (9) is feasible. Theorem 2 provides two fundamental operational regimes depending on the hotspot location relative to the macrocell.

Cellular-limited regime. A necessary condition for a positive femtocell contention density at distance D is $\mathcal{I}_{\frac{\kappa}{\kappa+1}}(T_f - U_f + 1, U_c) < \epsilon$, or $\kappa(D)$ in (4) is upper bounded as

$$\kappa \leq \frac{\mathcal{I}^{-1}(\epsilon, T_f - U_f + 1, U_c)}{1 - \mathcal{I}^{-1}(\epsilon, T_f - U_f + 1, U_c)}.$$

From Theorem 1, violating this condition implies that the hotspot cannot guarantee reliable coverage because of cross-tier interference.

Hotspot-limited regime. As $\kappa \rightarrow 0$ or $D^{-\alpha_c} \rightarrow 0$, the SIR at any femtocell located at D is primarily influenced by hotspot interference. Consequently, $\lambda_f^*(D)$ in (10) approaches the limit $\check{\lambda}_f$ given as

$$\check{\lambda}_f = \lim_{\kappa \rightarrow 0} \lambda_f^*(D) = \frac{\epsilon \check{\mathcal{K}}_f}{\mathcal{C}_f(\mathcal{Q}_f\beta)^{\delta_f}}, \text{ where } \check{\mathcal{K}}_f = \lim_{\kappa \rightarrow 0} \mathcal{K}_f = \left[1 + \sum_{l=1}^{T_f-U_f} \frac{1}{l!} \prod_{m=0}^{l-1} (m - \delta_f) \right]^{-1} \quad (13)$$

The limit $\check{\mathcal{K}}_f$ determines the maximum contention density in the special case of an *ad hoc* network—no cellular interference—of homogeneously distributed transmitters equipped with multiple antennas [16].

Their work shows that $\check{\mathcal{K}}_f$ and \mathcal{C}_f scales with T_f and U_f as

$$\check{\mathcal{K}}_f \sim \Theta[(T_f - U_f + 1)^{\delta_f}], \quad \mathcal{C}_f \mathcal{Q}_f^{\delta_f} \sim \Theta(U_f^{\delta_f}) \quad (14)$$

Further, $\forall \kappa \geq 0, \mathcal{K}_f \leq \check{\mathcal{K}}_f$ and \mathcal{K}_f is bounded as $(T_f - U_f + 1)^{\delta_f} \leq \check{\mathcal{K}}_f \leq \Gamma(1 - \delta_f)(T_f - U_f + 1)^{\delta_f}$ [16]. We shall now consider two cases in the hotspot-limited regime ($D^{-\alpha_c} \rightarrow 0$). First, with multiuser transmission to $U_f = T_f$ femtocell users and using (14), the femtocell area spectral efficiency (in b/s/Hz/m²) which is given as $(1 - \epsilon)U_f \check{\lambda}_f \log_2(1 + \beta)$ scales according to $\Theta(T_f^{1-\delta_f})$. With SU transmission, the ASE scales as $\Theta(T_f^{\delta_f})$. This suggests that in path loss regimes with $\alpha_{fo} < 4$, higher spatial reuse is obtainable (order-wise) provided femtocells employ their antennas to transmit to just one user. In contrast, MU femtocell transmission provides higher network-wide spatial reuse (order-wise) only when hotspot interference is significantly diminished ($\alpha_{fo} > 4$).

B. SIR Analysis at a Cellular User

We now consider a reference cellular user 0 at distance D from their macrocell B_0 . During a given signaling interval, neglecting background noise, the received signal at user 0 is then given as

$$y_0 = \sqrt{A_c} D^{-\frac{\alpha_c}{2}} \mathbf{h}_0^\dagger \mathbf{V} \mathbf{s} + \sqrt{A_{c,f}} \sum_{F_j \in \Pi_f} \mathbf{e}_j^\dagger \mathbf{W}_j \mathbf{r}_j |X_j|^{-\frac{\alpha_{fo}}{2}} \quad (15)$$

where $\mathbf{s} \in \mathbb{C}^{U_c \times 1}$, $\mathbb{E}[||\mathbf{s}||^2] \leq P_c$ and $\mathbf{r}_j \in \mathbb{C}^{U_f \times 1}$, $\mathbb{E}[||\mathbf{r}_j||^2] \leq P_f$ represent the transmit data symbols for users in each tier. Further, $|X_j|$ and $\mathbf{e}_j \in \mathbb{C}^{T_c \times 1}$ respectively denote the distance and the downlink vector channel from the interfering femtocell F_j to user 0. The received SIR for user 0 is given as

$$\text{SIR}_c(B_0, D) = \frac{\frac{P_c}{U_c} A_c D^{-\alpha_c} ||\mathbf{h}_0||^2}{\frac{P_f}{U_f} A_{c,f} \sum_{F_j \in \Pi_f} ||\mathbf{e}_j^\dagger \mathbf{W}_j||^2 |X_j|^{-\alpha_{fo}}} \quad (16)$$

For successfully decoding user 0's signal, $\text{SIR}_c(B_0, D)$ should be greater than equal to the minimum SIR target β . Define $\mathcal{Q}_c = U_c \frac{P_f}{P_c} \frac{A_{c,f}}{A_c} D^{\alpha_c}$. Then, the probability of successful reception at 0 is given as

$$\mathbb{P}[\text{SIR}_c(B_0, D) \geq \beta] = \mathbb{P}\left[\frac{||\mathbf{h}_0||^2}{\frac{1}{U_f} \sum_{F_j \in \Pi_f} ||\mathbf{e}_j^\dagger \mathbf{W}_j||^2 |X_j|^{-\alpha_{fo}}} \geq \mathcal{Q}_c \beta\right] \quad (17)$$

Both the desired channel powers denoted as $||\mathbf{h}_0||^2$ and the interfering marks [23] given by $||\mathbf{e}_j^\dagger \mathbf{W}_j||^2$ follow a chi-squared distribution with $2(T_c - U_c + 1)$ and $2U_f$ degrees of freedom respectively. Using [16], the maximum femtocell contention density $\lambda_f(D)$ for which (17) satisfies the maximum outage probability constraint $\mathbb{P}(\text{SIR}_c(B_0, D) \geq \beta) \geq 1 - \epsilon$ of a cellular user is given as

$$\lambda_f^*(D) = \frac{\epsilon \mathcal{K}_c}{\mathcal{C}_f (\mathcal{Q}_c \beta)^{\delta_f}}, \quad \text{where } \mathcal{K}_c = \left[1 + \sum_{j=1}^{T_c - U_c} \frac{1}{j!} \prod_{k=0}^{j-1} (k - \delta_f)\right]^{-1} \quad (18)$$

where $\delta_f = 2/\alpha_{fo}$ as before and \mathcal{C}_f is given by (11). From [16], \mathcal{K}_c is bounded as

$$(T_c - U_c + 1)^{\delta_f} \leq \mathcal{K}_c \leq \Gamma(1 - \delta_f) (T_c - U_c + 1)^{\delta_f} \quad (19)$$

where the upper bound is a good approximation for \mathcal{K}_c ; for example, with $T_c = 4$, $U_c = 1$ and $\alpha_{fo} = 3.8$, the term \mathcal{K}_c equals 3.47 while the upper bound equals 3.87.

Remark 3: Since (18) varies as $\mathcal{K}_c/U_c^{\delta_f}$, approximating \mathcal{K}_c by the upper bound in (19) shows that the maximum contention density for single user beamforming given as $\lambda_{f,SU}^*(D)$ is proportional to $\Gamma(1 - \delta_f)T_c^{\delta_f}$. With $1 < U_c < T_c$ transmitted users, the maximum femtocell contention density denoted as $\lambda_{f,MU}^*(D)$ is proportional to $\Gamma(1 - \delta_f)(T_c - U_c + 1)^{\delta_f}/U_c^{\delta_f}$. Therefore, SU transmission increases the maximum hotspot density by a factor of $[T_c U_c / (T_c - U_c + 1)]^{\delta_f}$. With $U_c = T_c$ users (implying $\mathcal{K}_c = 1$), one obtains $\lambda_{f,MU}^*(D)$ to be proportional to $T_c^{-\delta_f}$, so that $\lambda_{f,SU}^*(D)/\lambda_{f,MU}^*(D)$ equals $\Gamma(1 - \delta_f)T_c^{2\delta_f}$.

Given an average of λ_f femtocells per sq. meter, inverting (18) yields the maximum distance up to which the cellular outage probability lies below ϵ . This cellular coverage radius D_c is given as

$$D_c = \left(\frac{1}{\beta U_c} \frac{A_c}{A_{c,f}} \frac{P_c}{P_f} \right)^{1/\alpha_c} \left(\frac{\epsilon \mathcal{K}_c}{\lambda_f \mathcal{C}_f} \right)^{\frac{1}{\delta_f \alpha_c}} \quad (20)$$

Remark 4: Since D_c varies as $(P_c/P_f)^{1/\alpha_c}$, increasing the cellular coverage radius by a factor of k necessitates increasing P_c by $10\alpha_c \log_{10} k$ decibels relative to P_f .

Remark 5: In (20), D_c is proportional to $(\frac{\mathcal{K}_c^{1/\delta_f}}{U_c})^{\frac{1}{\alpha_c}}$. With SU transmission [resp. MU transmission to $U_c = T_c$ users] at the macrocell and applying (19), the cellular coverage distance D_c scales with T_c as $D_{c,SU} \sim \Theta(T_c^{1/\alpha_c})$, $D_{c,MU} \sim \Theta(T_c^{-1/\alpha_c})$. This suggests that SU macrocell transmission provides coverage improvement by a factor of T_c^{2/α_c} (order-wise) relative to MU transmission.

C. Design Interpretations

In this section, we provide design interpretations of the preceding results in realistic path loss scenarios. We shall use the system parameters given in Table I and the path loss model described in Section II-A.

Figure 3 plots the normalized no-coverage femtocell radius D_f versus P_f/P_c on a log-log scale considering both SU and MU femtocell transmission. In this context, D_f designates the minimum macrocell-femtocell distance necessary in order to tolerate cellular interference and hotspot interference from an average of N_f femtocells/cellsite. Two cases are considered namely a lightly loaded [resp. heavily loaded] femtocell network with $N_f = 1$ [resp. $N_f = 100$] femtocells/cellsite. Figs. 4-5 plot

the maximum number of simultaneous femtocell transmissions given as $\pi R_c^2 \lambda_f^*(D)$ considering SU and MU femtocell transmissions and different values of α_{fo} . Shown below are the three key observations.

Coverage improvement. In the cellular-limited regime with $T_f = 2$ antennas, Fig. 4 shows that SU transmission obtains a nearly 1.5x reduction in the no-coverage femtocell radius D_f w.r.t single antenna transmission. Next, both Figs. 3-4 show that SU transmission reduces D_f by a factor of nearly 1.8x relative to MU transmission. Both these observations agree with the predicted improvements in Corollary 1. This indicates that SU transmission significantly improves hotspot coverage.

Dominance of cellular interference. Fig. 3 shows overlapping no-coverage radii with $N_f = 1$ and $N_f = 100$ femtocells/cell-site irrespective of the transmission strategy. Similarly, in Figs. 4-5, N_f increases from zero (at the no-coverage femtocell radius) to greater than 100 femtocells per cell-site within a few meters outside the no-coverage radius. This step-like transition from the cellular-limited to the hot-spot limited regime suggests that cross-tier cellular interference is the capacity-limiting factor even in densely populated femtocell networks and interference between femtocells is negligible because of the proximity of home users to their APs and double wall partition losses.

Spatial Reuse. In the hotspot-limited regime with $\alpha_{fo} = 3.8$, SU transmission consistently outperforms MU transmission. For example, with $T_f = 2$ antennas, there is a nearly 1.7x spatial reuse gain ($N_f U_f = 1080$ with SU transmission versus $N_f U_f = 640$ with MU transmission). Next, Fig. 5 shows that MU transmission to $U_f = 2$ hotspot users provides a marginally higher spatial reuse relative to SU transmission which occurs only when hotspot interference is significantly diminished ($\alpha_{fo} = 4.8$). The conclusion is that SU femtocell transmission offers superior spatial reuse and MU performance suffers due to residual interference in realistic path loss scenarios.

Fig. 6 plots the maximum number of transmitting femtocells $N_f = \pi R_c^2 \lambda_f^*(D)$ as a function of the cellular user distance D . With $(P_c/P_f)_{\text{dB}} = 20$ and a desired $N_f = 60$ femtocells/cell-site, SU macrocell transmission provides a normalized cellular coverage radius $D_c \approx 0.35$. In contrast, the coverage provided by MU transmission is only $D_c \approx 0.13$, resulting in a coverage loss of 2.7x relative to SU transmission (Remark 5 gives an order-wise loss of $\Theta(T_c^{\delta_f}) = 2.07$).

In addition, with SU transmission and $(P_c/P_f)_{\text{dB}} = 0$, a cellular user at $D = 0.1$ can tolerate interference from nearly $N_f = 62$ femtocells/cell-site. In contrast, with MU transmission, N_f reduces to nearly 8 femtocells/cell-site. The observed improvement in the maximum femtocell contention density (equaling 7.75x) is well approximated by the predicted improvement ($\Gamma(1 - \delta_f) T_c^{2\delta_f} = 8.04\text{x}$) in Remark 3.

The preceding observations reveal 1) since MU performance is significantly limited by cross-tier interference, the macrocell and femtocell should maximize their coverage by transmitting to just a

single user and 2) that femtocells should regulate their transmit powers for ensuring reliable cellular coverage.

IV. INTERFERENCE MANAGEMENT USING CARRIER-SENSING AT FEMTOCELLS

To motivate carrier-sensing at femtocells, Fig. 4 shows that even with $(P_c/P_f)_{\text{dB}} = 20$, a femtocell at normalized distance $D = 0.4$ can tolerate hotspot interference from greater than 1000 neighboring femtocells. This suggests that in dense femtocell deployments (eg. 60 femtocells in a radius of $R_c = 1$ km), $(P_c/P_f)_{\text{dB}}$ can be increased to minimize hotspot interference without violating the QoS requirement at femtocells. This section presents a carrier-sensing interference management strategy for choosing the femtocell transmission power provided there is a cellular user in its vicinity.

AS 3: Each cellular user periodically transmits over a set of uplink pilot slots (time or frequency resource) with power $P_{\text{UT,pilot}}$ for communicating their channel information to the macrocell.

AS 4: Each femtocell is capable of inferring its distance from its closest macrocell.

During carrier-sensing, each femtocell performs energy detection while monitoring uplink pilot cellular transmissions. In the absence of a cellular user, the femtocell maintains a constant transmit power P_f . When the detected energy of a cellular user exceeds a threshold, the femtocell chooses its P_f based on its location D within the underlying macrocell.

A. Minimum Required Sensing Range and Per-Tier Transmit Power Ratio Bounds

We shall first derive the minimum required sensing distance D_{sense} such that any transmitting femtocell located within $R < D_{\text{sense}}$ meters of the cellular user violates its maximum outage probability requirement. Define the notation $\mathcal{B}(D_{\text{sense}})$ to denote a circular region of radius D_{sense} containing $|\mathcal{B}(D_{\text{sense}})|$ femtocells. Given an intensity of λ_f femtocells per square meter and assuming the cellular user 0 is located at normalized distance D w.r.t the macrocell, its outage probability is lower bounded as

$$\begin{aligned} \mathbb{P}[\text{SIR}_c(B_0, D) \leq \beta] &\stackrel{(a)}{\geq} \mathbb{P}[\text{SIR}_c(B_0, D) \leq \beta, |\mathcal{B}(D_{\text{sense}})| > 0] \\ &\stackrel{(b)}{=} \mathbb{P} \left[\text{SIR}_c(B_0, D) \leq \beta \mid |\mathcal{B}(D_{\text{sense}})| > 0 \right] \cdot (1 - e^{-\lambda_f \pi D_{\text{sense}}^2}) \\ &\stackrel{(c)}{>} \mathbb{P} \left[\text{SIR}_c(B_0, D) \leq \beta \mid |\mathcal{B}(D_{\text{sense}})| = 1, R = D_{\text{sense}} \right] \cdot (1 - e^{-\lambda_f \pi D_{\text{sense}}^2}) \end{aligned} \quad (21)$$

where step (a) in (21) is a lower bound as it ignores the event of zero hotspots present within $\mathcal{B}(D_{\text{sense}})$. Step (b) rewrites (a) in terms of the conditional probability. Finally, step (c) is a lower bound because it considers the event that $|\mathcal{B}(D_{\text{sense}})| = 1$ and the hotspot is located exactly at $R = D_{\text{sense}}$ meters (thereby experiencing the highest path loss). A necessary condition for ensuring $\mathbb{P}[\text{SIR}_c(B_0, D) \leq \beta] \leq \epsilon$ is

that the right hand side in step (c) in (21) consisting of the product of two probabilities should be less than ϵ . The first term represents the outage probability from interfering hotspots due to the time-varying channel powers and the second term represents the probability that $\mathcal{B}(D_{\text{sense}})$ is non-empty.

Assuming large λ_f (or $1 - e^{-\lambda_f \pi D_{\text{sense}}^2} \rightarrow 1$), a reasonable choice for selecting D_{sense} is to set the conditional outage probability $\mathbb{P} \left[\text{SIR}_c(B_0, D) \leq \beta \mid |\mathcal{B}(D_{\text{sense}})| = 1, R = D_{\text{sense}} \right]$ to equal ϵ . Evaluating this probability,

$$\begin{aligned} \mathbb{P} \left[\frac{\frac{P_c}{U_c} A_c D^{-\alpha_c} \|\mathbf{h}_0\|^2}{\frac{P_f}{U_f} A_{c,f} \|\mathbf{g}_0\|^2 D_{\text{sense}}^{-\alpha_{f_o}}} \leq \beta \right] &= \mathbb{P} \left[\frac{\|\mathbf{h}_0\|^2}{\|\mathbf{g}_0\|^2} \leq \frac{\beta Q_c D_{\text{sense}}^{-\alpha_{f_o}}}{U_f} \right] \\ &\stackrel{(a)}{=} \mathbb{P} \left[Z \leq \theta \frac{U_f}{T_c - U_c + 1} \right] \\ &\stackrel{(b)}{=} \mathcal{I}_{\frac{\theta}{\theta+1}}(T_c - U_c + 1, U_f) \end{aligned} \quad (22)$$

where $Q_c = U_c \frac{P_f}{P_c} \frac{A_{c,f}}{A_c} D^{\alpha_c}$ as before, while $\|\mathbf{h}_0\|^2 \sim \chi_{2(T_c - U_c + 1)}^2$ and $\|\mathbf{g}_0\|^2 \sim \chi_{2U_f}^2$ denote the chi-squared distributed desired and interfering channel powers respectively in (22). Step (a) in (22) follows by defining $\theta \triangleq Q_c \beta D_{\text{sense}}^{-\alpha_{f_o}} / U_f$ and defining the normalized ratio $Z = \frac{\|\mathbf{h}_0\|^2 / (T_c - U_c + 1)}{\|\mathbf{g}_0\|^2 / U_f}$ which is F-distributed [36]. Step (b) follows by substituting the cdf of the F-distributed r.v Z . The minimum required sensing radius at D is consequently given as

$$D_{\text{sense}} \geq \left[\left(\frac{Q_c \beta}{U_f} \right) \left(\frac{1 - \mathcal{I}^{-1}(\epsilon; T_c - U_c + 1, U_f)}{\mathcal{I}^{-1}(\epsilon; T_c - U_c + 1, U_f)} \right) \right]^{1/\alpha_{f_o}} \quad (23)$$

Using the numerical values in Table I, Fig. 8 plots D_{sense} for different values of the path loss exponents α_c and α_{f_o} as well as different cellular user locations D . Assuming SU transmission in both tiers, $(P_c/P_f)_{\text{dB}} = 20$ dB and $\alpha_c = \alpha_{f_o} = 3.8$, a minimum sensing range $D_{\text{sense}} \approx 160$ meters is required at the cell-edge ($D = R_c$).

Next, the following lemma derives bounds on P_c/P_f that satisfy the per-tier outage probability requirements at distance D from the macrocell.

Lemma 1: Given a mean intensity of λ_f femtocells per square meter and minimum per-tier SIR target β , satisfying the per-tier outage probability requirement at distance D from the macrocell necessitates (P_c/P_f) to be bounded as $(P_c/P_f)_{\text{lb}}[D] \leq P_c/P_f \leq (P_c/P_f)_{\text{ub}}[D]$, which are given as

$$\left(\frac{P_c}{P_f} \right)_{\text{lb}} [D] = \beta \left(\frac{A_{c,f}}{A_c} \right) \left(\frac{U_c}{D^{-\alpha_c}} \right) \left(\frac{C_f \lambda_f}{\epsilon \mathcal{K}_c} \right)^{1/\delta_f} \quad (24)$$

$$\left(\frac{P_c}{P_f} \right)_{\text{ub}} [D] = \left(\frac{1}{\beta} \right) \left(\frac{A_{f,i}}{A_{f,c}} \right) \left(\frac{U_c R_f^{-\alpha_{f,i}}}{U_f D^{-\alpha_c}} \right) \frac{\mathcal{I}^{-1}(\tilde{\epsilon}; T_f - U_f + 1, U_c)}{1 - \mathcal{I}^{-1}(\tilde{\epsilon}; T_f - U_f + 1, U_c)} \quad (25)$$

where $\delta_f = 2/\alpha_{f_o}$ as before, \mathcal{K}_c is given by (18), \mathcal{Q}_f is given by (2), \mathcal{C}_f is given by (11) and

$$\tilde{\epsilon} = \frac{\epsilon - \lambda_f \mathcal{C}_f(\mathcal{Q}_f \beta_f)^{\delta_f} / \mathcal{K}_f}{1 - \lambda_f \mathcal{C}_f(\mathcal{Q}_f \beta_f)^{\delta_f}} \text{ and } K_f \leq (T_f - U_f + 1)^{\delta_f} \Gamma(1 - \delta_f) \quad (26)$$

Proof: A lower limit on P_c/P_f is obtained by computing the minimum P_c required to satisfy the outage probability requirement for a cellular user at distance D . Combining (18) and (19) yields $(P_c/P_f)_{\text{lb}}$ in (24). Conversely, given a cellular transmit power P_c , an upper limit for P_c/P_f is obtained by computing the minimum required P_f for satisfying $\mathbb{P}[\text{SIR}(F_0, D) \leq \beta] \leq \epsilon$. Substituting the upper bound for \mathcal{K}_f and inverting (10) to compute $(P_c/P_f)_{\text{ub}}$ yields (25). ■

The lower bound $(P_c/P_f)_{\text{lb}}[D]$ in (24) considers D as the distance of a cellular user from their macrocell. Conversely, $(P_c/P_f)_{\text{ub}}[D]$ considers D as the distance of the reference femtocell from the macrocell. Inspecting (24) and (25) reveals that the difference between the decibel upper and lower bounds is constant for all D . Fig. 7 plots $(P_c/P_f)_{\text{lb}}$ and $(P_c/P_f)_{\text{ub}}$ at different distances D from the macrocell. As an example, for a cell-edge ($D = 1$) location, the bounds on the required $(P_c/P_f)_{\text{dB}}$ are given as $40 \leq (P_c/P_f)_{\text{dB}} \leq 55$ dB.

B. Energy Detection based Carrier-Sensing of Cellular Users

Assume that each femtocell monitors a set of pilot slots (we assume time-slotted transmission in the subsequent discussion) and employs energy detection [32]. We briefly describe the sensing procedure below and refer to [18], [21], [32], [33] for further details.

Let T denote the sensing time (number of sensing time slots times the slot duration) and W designate the sensed bandwidth. Given a received signal $x(t)$ in the pilot slots and $n(t)$ being complex Gaussian noise process with power $N_0W/2$ per complex dimension, define the following hypotheses namely 1) \mathcal{H}_0 : Absence of cellular user [$x(t) = n(t)$] and 2) \mathcal{H}_1 : Presence of an active cellular user [$x(t) = hs(t) + n(t)$]. The femtocell compares the energy detector output $Y = 2/N_0 \int_0^T |x(t)|^2 dt$ against a threshold λ for inferring the presence (or absence) of a cellular user. Define m to equal the time-bandwidth product TW (assumed to be an integer). The average sensed pilot Signal-to-Noise Ratio (SNR) at the femtocell is given as

$$\bar{\gamma} = \frac{P_{\text{UT,pilot}} D^{-\alpha_c} A_{f,c}}{N_0 W}, \text{ where } (N_0 W)_{\text{dB}} = P_{c,\text{dB}} - A_{c,\text{dB}} - 10\alpha_c \log_{10}(R_c) - \bar{\gamma}_{\text{edge,dB}} \quad (27)$$

where D denotes the distance of the cellular user from the femtocell. The noise power N_0W is chosen with reference to a cell-edge user obtaining an average downlink SNR $\bar{\gamma}_{\text{edge}} > \beta$. Assuming Selection Combining (SC) is used at the T_f available diversity branches for choosing the maximum SNR branch,

the detection probability $P_{d,SC}$ and the false-alarm probability P_f are respectively given as [21], [33]

$$P_{d,SC} = \mathbb{P}[Y > \lambda | \mathcal{H}_1] = T_f \cdot \sum_{i=0}^{T_f-1} \frac{(-1)^i}{i+1} \binom{T_f-1}{i} P_{d, \text{Ray}} \left(\frac{\bar{\gamma}}{i+1} \right), P_f = \mathbb{P}[Y > \lambda | \mathcal{H}_0] = \frac{\Gamma(2m, \lambda)}{\Gamma(2m)}$$

$$\text{where } P_{d, \text{Ray}}(\bar{\gamma}) = \frac{\Gamma(2m-1, \lambda)}{\Gamma(2m-1)} + e^{-\frac{\lambda}{(1+m\bar{\gamma})}} \left(1 + \frac{1}{m\bar{\gamma}} \right)^{2m-1} \left[1 - \frac{\Gamma(2m-1, \frac{\lambda m \bar{\gamma}}{(1+\lambda m \bar{\gamma})})}{\Gamma(2m-1)} \right] \quad (28)$$

where $\Gamma(a, x) = \int_x^\infty t^{a-1} e^{-t} dt$ is the upper incomplete gamma function. Because of the complex baseband signal model, there is a factor of 2 discrepancy in (28) with respect to [21]. Fig. 9 plots the maximum femtocell sensing range D_{sense} versus different values of the time-bandwidth product m . For example, with $P_{\text{UT}, \text{pilot}} = 20$ dBm (3 dB below the maximum UT transmit power), and target probabilities $P_d = 0.9$ and $P_f = 0.1$ respectively, obtaining a sensing range of $D_{\text{sense}} = 230$ meters requires a minimum time-bandwidth product $m = 500$.

V. NUMERICAL RESULTS

This section reports the results of computer simulations using the system parameters in Table I. The simulation consisted of 1000 different random drops of femtocell hotspots with 1000 trials per drop to simulate Rayleigh fading. Additive white Gaussian noise power was chosen to obtain an average cell-edge SNR of $\bar{\gamma}_{\text{edge, dB}} = 12$ dB. Single-user transmission is assumed in either tier considering its superior coverage and spatial reuse performance. With an average of $N_f = 60$ femtocells per cell-site, we evaluate whether the 10 percentile outage capacity ($\epsilon = 0.1$) satisfies the minimum required per-tier spectral efficiency $\log_2(1 + \beta)$ b/s/Hz (or nearly 2.06 b/s/Hz for $\beta_{\text{dB}} = 5$).

During carrier-sensing, each femtocell can detect active cellular users within a sensing radius equaling 230 meters (determined using computer simulations), which exceeds the minimum required sensing range of $D_{\text{sense}} = 160$ meters. We consider both a fixed P_c/P_f (without carrier-sensing or power control at femtocells) and a location based selection of P_c/P_f (wherein femocells adjust their P_f upon sensing a cellular user). Under ambient conditions (no detected cellular user), a fixed $(P_c/P_f)_{\text{dB}} = 20$ dB is chosen. Upon sensing a cellular user, a femtocell chooses its P_f such that $(P_c/P_f)[D, \text{dB}] = 0.7(P_c/P_f)_{\text{ub}}[D, \text{dB}] + 0.3(P_c/P_f)_{\text{lb}}[D, \text{dB}]$, which are given in (24)-(25). Two scenarios are considered namely

Reference Cellular User. A cellular user is placed at normalized distances ($D = 0.8$ and $D = 1.0$) w.r.t the macrocell. The cdfs of the achievable cellular data rates have been reported.

Reference Hotspot. A reference hotspot is placed at normalized distances ($D = 0.11, 0.4, 0.6, 0.8$ and 0.9 respectively) from the macrocell. A reference cellular user is co-linearly placed at a distance

$D_{\text{sense}}/2$ w.r.t the hotspot. The conditional cdfs of the hotspot data rates (assuming idealized sensing) have been reported.

Fig. 10 shows the cdfs of the obtained cellular data rates for $N_f = 60$ femtocells/cell-site. Without carrier-sensing, the 10 percentile outage capacities are below 0.5 b/s/Hz. By employing carrier-sensing, the 10 percentile outage capacities (corresponding to $\epsilon = 0.1$) equal 3.21 b/s/Hz and 2.22 b/s/Hz for cellular user locations of $D = 0.8$ and $D = 1.0$ respectively. Thus, our scheme ensures uniform cell-edge coverage with large numbers of femtocells.

Fig. 11 shows the cdfs of the obtained hotspot data rates with carrier-sensing and transmit power control at hotspots. The lowest outage capacity is obtained when the femtocell is located close to the no-coverage zone ($D = 0.11$). Because of the location-based power control at femtocells, the outage capacities monotonically decrease with increasing hotspot distance to the macrocell. The 10 percentile hotspot outage capacities are respectively equal to 2.15, 3.63, 3.56, 3.32 and 3.22 b/s/Hz for the different hotspot locations given above which exceeds the minimum desired target spectral efficiency of 2.06 b/s/Hz.

VI. CONCLUSIONS

In two-tier cellular systems with universal frequency reuse, cross-tier interference will likely be the main obstacle preventing uniform coverage. This paper has derived analytical expressions for the coverage zones in such a tiered architecture with spatial diversity considering the number of antennas, the maximum tolerable outage probability accounting for path loss and Rayleigh fading. Single-user transmission in either tier is analytically shown to provide significantly superior coverage and spatial reuse while performance of multiple-user transmission suffers from residual cross-tier interference. For providing uniform cellular coverage, we have proposed a location-assisted power control scheme for regulating femtocell transmit powers. This scheme is fully decentralized and provides uniform cellular and hotspot coverage on the cell-edge, as opposed to randomized hotspot transmissions without carrier-sensing. These results motivate deploying closed-access tiered cellular architectures while requiring minimal network overhead.

APPENDIX I

PROOF OF THEOREM 1

The probability of successful reception in (3) can be upper bounded as

$$\mathbb{P}[\text{SIR}_f(F_0, D) \geq \beta] \leq \mathbb{P}\left[\|\mathbf{g}_0\|^2 \geq \beta \mathcal{Q}_f \left(\frac{\mathcal{P}_f}{U_c} \|\mathbf{f}_0^\dagger \mathbf{V}\|^2 \right)\right] \quad (29)$$

The term $\|\mathbf{g}_0\|^2$ is distributed as a chi-squared random variable (r.v) X with $2(T_f - U_f + 1)$ degrees of freedom [34], [35] denoted as $\chi_{2(T_f - U_f + 1)}^2$. The probability density function of $\|\mathbf{g}_0\|^2$ is given as $f_{\|\mathbf{g}_0\|^2}(x) = x^{T_f - U_f} e^{-x} / \Gamma(T_f - U_f + 1) \forall x \geq 0$ where $\Gamma(k) = (k - 1)!$ for any positive integer k .

Similarly, the r.v $\|\mathbf{f}_0^\dagger \mathbf{V}\|^2 = \sum_{k=0}^{U_c-1} |\mathbf{f}_0^\dagger \mathbf{v}_k|^2$ is the sum of U_c r.v's, wherein each term $|\mathbf{f}_0^\dagger \mathbf{v}_k|^2$ equals the squared modulus of a linear combination of T_c complex normal r.v's, which is exponentially distributed. Consequently, $\|\mathbf{f}_0^\dagger \mathbf{V}\|^2$ is distributed as a $\chi_{2U_c}^2$ r.v.

Define $Z = \frac{\|\mathbf{g}_0\|^2}{\|\mathbf{f}_0^\dagger \mathbf{V}\|^2}$. Then Z is the ratio of two independent χ^2 r.v's with $2(T_f - U_f + 1)$ and $2U_c$ degrees of freedom respectively. Therefore, Z follows a canonical F_c -distribution [36] and $\frac{Z U_c}{(T_f - U_f + 1)}$ is an F-distributed r.v with parameters $2(T_f - U_f + 1)$ and $2U_c$ respectively. Substituting κ in (4) and taking the complement of (29), one obtains

$$\mathbb{P}[\text{SIR}_f(F_0, D) \leq \beta] \geq \mathbb{P}[Z \leq \kappa] = \mathbb{P}\left[\frac{Z U_c}{T_f - U_f + 1} \leq \kappa \frac{U_c}{T_f - U_f + 1}\right] = \mathcal{I}_{\frac{\kappa}{\kappa+1}}(T_f - U_f + 1, U_c) \quad (30)$$

A necessary condition to ensure successful reception at indoor users served by F_0 is given as

$$\mathcal{I}_{\frac{\kappa}{\kappa+1}}(T_f - U_f + 1, U_c) \leq \epsilon \Rightarrow \kappa^* = \frac{\mathcal{I}^{-1}(\epsilon; T_f - U_f + 1, U_c)}{1 - \mathcal{I}^{-1}(\epsilon; T_f - U_f + 1, U_c)} \quad (31)$$

Substituting the definition of κ in (4), one obtains D_f . This completes the proof.

APPENDIX II

Using (3), the probability of successful reception $\mathbb{P}[\text{SIR}_f(F_0, D) \geq \beta]$ is given as

$$\mathbb{P}[\|\mathbf{g}_0\|^2 \geq \beta \mathcal{Q}_f(I_{f,c} + I_{f,f})], \quad I_{f,c} = \frac{\mathcal{P}_f}{U_c} \|\mathbf{f}_0^\dagger \mathbf{V}\|^2, \quad I_{f,f} = \frac{1}{U_f} \sum_{F_j \in \Pi_f \setminus F_0} \|\mathbf{g}_{0,j}^\dagger \mathbf{W}_j\|^2 |X_{0,j}|^{-\alpha_{f_0}} \quad (32)$$

The interference from neighboring femtocells $I_{f,f}$ is a Poisson Shot-noise Process [37], [38] with independent and identically distributed marks [23]. The distributions of the signal powers and marks of the interferers are chi-squared with degrees of freedom given as $\|\mathbf{g}_0\|^2 \sim \chi_{2(T_f - U_f + 1)}^2$, $\|\mathbf{f}_0^\dagger \mathbf{V}\|^2 \sim \chi_{2U_c}^2$ and $\|\mathbf{g}_{0,j}^\dagger \mathbf{W}_j\|^2 \sim \chi_{2U_f}^2$ respectively. Consequently,

$$\mathbb{P}[\text{SIR}_f(F_0, D) \geq \beta] \stackrel{(a)}{=} \int_0^\infty \sum_{k=0}^{T_f - U_f} \frac{(s \mathcal{Q}_f \beta)^k}{k!} e^{-s \mathcal{Q}_f \beta} \mathbf{d}\mathbb{P}(I_{f,c} + I_{f,f} \leq s) \quad (33)$$

$$\stackrel{(b)}{=} \sum_{k=0}^{T_f - U_f} \frac{(-\mathcal{Q}_f \beta)^k}{k!} \frac{\mathbf{d}^k}{\mathbf{d}\theta^k} \mathcal{L}_{I_{f,c}}(\theta) \mathcal{L}_{I_{f,f}}(\theta) \Big|_{\theta = \mathcal{Q}_f \beta} \quad (34)$$

where step (a) follows by conditioning on $I_{f,c} + I_{f,f}$ and computing the complementary cumulative distribution (ccdf) of $\|\mathbf{g}_0\|^2$. For deriving step (b), with $k = 0$, the integral in (a) corresponds to the Laplace Transform (LT) of the r.v $I_{f,f} + I_{f,c}$ given as $\mathbb{E}[e^{-(I_{f,c} + I_{f,f})\theta}]$ evaluated at $\theta = \mathcal{Q}_f \beta$ (originally derived in [27]). Next, since $I_{f,c}$ and $I_{f,f}$ are independent r.v's, the LT of their sum decouples as

the product of their LTs $\mathbb{E}[e^{-I_{f,c}\theta}]\mathbb{E}[e^{-I_{f,f}\theta}]$. Finally, for any $k > 0$, we have the identity $\mathcal{L}[t^k f(t)] = (-1)^k F^{(k)}(s)$, where $F^{(k)}(s)$ represents the k th derivative of $F(s)$ (this technique is borrowed from [16]).

The LTs of $I_{f,c}$ and $I_{f,f}$ may be written as

$$\mathcal{L}_{I_{f,c}}(\theta) = \mathbb{E}[e^{-\theta I_{f,c}}] = \frac{1}{(1 + \mathcal{P}_f \theta / U_c)^{U_c}} \quad (35)$$

$$\begin{aligned} \mathcal{L}_{I_{f,f}}(\theta) &= \mathbb{E}[e^{-\theta I_{f,f}}] \stackrel{(a)}{=} \exp \left\{ -\lambda_f \int_{\mathbb{R}^2} 1 - \mathbb{E}_S[e^{-\theta \frac{S}{U_f} |x|^{-\alpha_{f_0}}}] dx \right\}, \text{ where } S \sim \chi_{2U_f}^2 \\ &\stackrel{(b)}{=} \exp \left\{ -\pi \lambda_f \delta_f \left(\frac{\theta}{U_f} \right)^{\delta_f} \sum_{k=0}^{U_f-1} \binom{U_f}{k} B(k + \delta_f, U_f - k - \delta_f) \right\} \\ &\stackrel{(c)}{=} \exp(-\lambda_f \mathcal{C}_f \theta^{\delta_f}) \end{aligned} \quad (36)$$

where (35) follows from the LT of a chi-squared r.v with $2U_c$ degrees of freedom. In (36), step (a) represents the LT of a Poisson Shot-Noise process with independent and identically distributed marks S_j -equaling $\|\mathbf{g}_{0,j}^\dagger \mathbf{W}_j\|^2$ in our case. Steps (b) and (c) follow from [16]. Substituting (35) and (36) in (34) leads to the following requirement for the success probability

$$\sum_{k=0}^{T_f - U_f} \frac{(-\mathcal{Q}_f \beta)^k}{k!} \frac{d^k}{d\theta^k} \frac{e^{-\lambda_f \mathcal{C}_f \theta^{\delta_f}}}{(1 + \frac{\mathcal{P}_f \theta}{U_c})^{U_c}} \geq 1 - \epsilon, \text{ where } \theta = \mathcal{Q}_f \beta \quad (37)$$

Using the Leibniz rule, the k th derivative of $\mathcal{L}_{I_{f,c}}(\theta)\mathcal{L}_{I_{f,f}}(\theta)$ is given as

$$\frac{d^k}{d\theta^k} \frac{e^{-\lambda_f \mathcal{C}_f \theta^{\delta_f}}}{(1 + \frac{\mathcal{P}_f \theta}{U_c})^{U_c}} = \sum_{j=0}^k \binom{k}{j} \frac{d^j}{d\theta^j} \left(1 + \frac{\mathcal{P}_f \theta}{U_c} \right)^{-U_c} \frac{d^{(k-j)}}{d\theta^{(k-j)}} e^{-\lambda_f \mathcal{C}_f \theta^{\delta_f}} \quad (38)$$

where $\binom{a}{b}$ is the coefficient of x^b in the expansion of $(1+x)^a$. Considering the low outage regime, we shall evaluate the k th derivative of $\mathcal{L}_{I_{f,f}}(\theta)$ using a first-order Taylor series approximation around $\lambda_f \mathcal{C}_f \theta^{\delta_f} = 0$. Then, for all $k \geq 1$, the k th derivatives of $\mathcal{L}_{I_{f,c}}(\theta)$ and $\mathcal{L}_{I_{f,f}}(\theta)$ are individually given as

$$\frac{d^k}{d\theta^k} \left(1 + \frac{\mathcal{P}_f \theta}{U_c} \right)^{-U_c} = \frac{\left[\prod_{j=0}^{k-1} (U_c + j) \right] \left(\frac{-\mathcal{P}_f}{U_c} \right)^k}{\left(1 + \frac{\mathcal{P}_f \theta}{U_c} \right)^{k+U_c}} \quad (39)$$

$$\frac{d^k}{d\theta^k} e^{-\lambda_f \mathcal{C}_f \theta^{\delta_f}} = - \left[\lambda_f \mathcal{C}_f \prod_{m=0}^{k-1} (\delta_f - m) \theta^{\delta_f - k} \right] e^{-\lambda_f \mathcal{C}_f \theta^{\delta_f}} + \Theta(\lambda_f^2 \mathcal{C}_f^2 \theta^{2\delta_f}) \quad (40)$$

Combining (37) with (39) and (40) and substituting $\theta = \mathcal{Q}_f \beta$ leads to

$$\begin{aligned} &\frac{e^{-\lambda_f \mathcal{C}_f (\mathcal{Q}_f \beta)^{\delta_f}}}{\left(1 + \frac{\mathcal{P}_f \mathcal{Q}_f \beta}{U_c} \right)^{U_c}} \left\{ \sum_{k=0}^{(T_f - U_f)} \frac{\left(\frac{\mathcal{P}_f \mathcal{Q}_f \beta}{U_c} \right)^k}{k! \left(1 + \frac{\mathcal{P}_f \mathcal{Q}_f \beta}{U_c} \right)^k} \prod_{m=0}^{(k-1)} (U_c + m) \right. \\ &- \lambda_f \mathcal{C}_f (\mathcal{Q}_f \beta)^{\delta_f} \sum_{k=1}^{(T_f - U_f)} \frac{(-1)^k}{k!} \sum_{j=1}^k \binom{k}{j} \left[\frac{-\mathcal{P}_f \mathcal{Q}_f \beta}{1 + \frac{\mathcal{P}_f \mathcal{Q}_f \beta}{U_c}} \right]^{k-j} \prod_{n=0}^{(k-j-1)} (U_c + n) \prod_{m=0}^{j-1} (\delta_f - m) \left. \right\} \\ &+ \Theta(\lambda_f^2 \mathcal{C}_f^2 (\mathcal{Q}_f \beta)^{2\delta_f}) \geq 1 - \epsilon \end{aligned}$$

Next, substituting $\kappa = \mathcal{P}_f \mathcal{Q}_f \beta / U_c$ from (4) and performing a first-order Taylor series expansion of $e^{-\lambda_f \mathcal{C}_f(\mathcal{Q}_f \beta)^{\delta_f}} = 1 - \lambda_f \mathcal{C}_f(\mathcal{Q}_f \beta)^{\delta_f} + \Theta(\lambda_f^2 \mathcal{C}_f^2(\mathcal{Q}_f \beta)^{2\delta_f})$, the above expression simplifies as

$$\begin{aligned} & \frac{1 - \lambda_f \mathcal{C}_f(\mathcal{Q}_f \beta)^{\delta_f}}{(1 + \kappa)^{U_c}} \left\{ \sum_{k=0}^{T_f - U_f} \frac{1}{k!} \left(\frac{\kappa}{\kappa + 1} \right)^k \prod_{m=0}^{k-1} (U_c + m) \right. \\ & - \lambda_f \mathcal{C}_f(\mathcal{Q}_f \beta)^{\delta_f} \sum_{k=1}^{T_f - U_f} \frac{1}{k!} \sum_{j=1}^k \binom{k}{j} \left[\frac{\kappa}{\kappa + 1} \right]^{k-j} \prod_{n=0}^{k-j-1} (U_c + n) \prod_{m=0}^{j-1} (m - \delta_f) \left. \right\} \\ & + \Theta(\lambda_f^2 \mathcal{C}_f^2(\mathcal{Q}_f \beta)^{2\delta_f}) \geq 1 - \epsilon \end{aligned} \quad (41)$$

Note that $\prod_{m=0}^{k-1} (U_c + m) / k! = \binom{U_c + k - 1}{k}$. Using Proposition 2, we have the identity

$$\sum_{k=0}^{(T_f - U_f)} \left(\frac{\kappa}{\kappa + 1} \right)^k \binom{U_c + k - 1}{k} = (1 + \kappa)^{U_c} [1 - \mathcal{I}_{\frac{\kappa}{\kappa+1}}(T_f - U_f + 1; U_c)] \quad (42)$$

With straightforward algebraic manipulation, it is easily shown that

$$\begin{aligned} & \sum_{k=1}^{(T_f - U_f)} \frac{1}{k!} \sum_{j=1}^k \binom{k}{j} \left[\frac{\kappa}{\kappa + 1} \right]^{k-j} \prod_{n=0}^{k-j-1} (U_c + n) \prod_{m=0}^{j-1} (m - \delta_f) \\ & = \sum_{j=0}^{T_f - U_f - 1} \left(\frac{\kappa}{\kappa + 1} \right)^j \binom{U_c + j - 1}{j} \sum_{l=1}^{T_f - U_f - j} \frac{1}{l!} \prod_{m=0}^{l-1} (m - \delta_f) \end{aligned} \quad (43)$$

Using (43), we now define \mathcal{K}_f in (12), where $\mathcal{K}_f = 1$ whenever $U_f = T_f$. By substituting (42) and \mathcal{K}_f in (41) and dropping the $\Theta(\lambda_f^2)$ terms, the upper bound on λ_f is given as

$$\lambda_f \leq \frac{1}{\mathcal{C}_f(\mathcal{Q}_f \beta)^{\delta_f}} \frac{\epsilon - \mathcal{I}_{\frac{\kappa}{\kappa+1}}(T_f - U_f + 1, U_c)}{\frac{1}{\mathcal{K}_f} - \mathcal{I}_{\frac{\kappa}{\kappa+1}}(T_f - U_f + 1, U_c)} \quad (44)$$

Since the *maximum contention density* λ_f^* maximizes the number of simultaneous femtocell transmissions, λ_f^* satisfies (44) with equality. This completes the proof.

APPENDIX III

Proposition 2: For any $x \geq 0$, and non-negative integers n, m and r where $n \geq r$,

$$\sum_{k=0}^{n-r} \left(\frac{x}{x+1} \right)^k \binom{m+k-1}{k} = (1+x)^m \mathcal{I}_{\frac{1}{x+1}}(m, n-r+1) \quad (45)$$

Proof: Multiplying the left hand side of (45) by $(1+x)^{n-r}$,

$$\sum_{k=0}^{n-r} x^k (1+x)^{n-r-k} \binom{m+k-1}{k} = \sum_{k=0}^{n-r} \sum_{l=0}^{n-r-k} \binom{n-r-k}{l} \binom{m+k-1}{k} x^{k+l} \quad (46)$$

The coefficient of x^q , where $0 \leq q \leq n - r$, is given as $\sum_{j=0}^q \binom{n-r-j}{q-j} \binom{m+j-1}{j} = \binom{n-r+m}{q}$ (using the combinatorial identity [39, Page 22, (3.2)]). Consequently, we have

$$\sum_{k=0}^{n-r} x^k (1+x)^{n-r-k} \binom{m+k-1}{k} = \sum_{k=0}^{n-r} \binom{n-r+m}{k} x^k \quad (47)$$

Next, by definition of the incomplete Beta function and using $\mathcal{I}_t(a, b) = 1 - \mathcal{I}_{1-t}(b, a)$,

$$(1+x)^m \mathcal{I}_{\frac{1}{x+1}}(m, n-r+1) \stackrel{(a)}{=} \sum_{j=m}^{n-r+m} \binom{n-r+m}{j} \frac{x^{n-r+m-j}}{(1+x)^{n-r}} \stackrel{(b)}{=} \sum_{k=0}^{n-r} \binom{n-r+m}{k} \frac{x^k}{(1+x)^{n-r}} \quad (48)$$

where step (a) follows by definition, while step (b) follows by replacing the index j in step (a) by $k = n - r + m - j$. Combining (47) and (48) gives the desired result. ■

TABLE I
SYSTEM PARAMETERS

Variable	Parameter	Sim. Value
β	Minimum per-tier SIR Target for successful reception	5 dB
$\bar{\gamma}_{\text{edge,dB}}$	Average SNR of cell-edge user	12 dB
ϵ	Maximum tolerable per-tier outage probability	10%
R_c	Macrocell Radius	1000 m
R_f	Femtocell Radius	30 m
T_c	Transmit Antennas at macrocell	4 antennas
T_f	Transmit Antennas at femtocell	2 antennas
P_c	Maximum Transmit Power at macrocell	43 dBm
P_f	Maximum Transmit Power at femtocell	23 dBm
P_{UT}	Maximum Transmit Power at User Terminal	23 dBm
P_{dB}	Indoor to Outdoor Wall Partition Loss	5 dB
f_c	Carrier Frequency	2000 MHz
α_c	Outdoor path loss exponent	3.8
α_{fo}	Indoor to Outdoor path loss exponent	3.8
α_{fi}	Indoor path loss exponent	3

REFERENCES

- [1] V. Chandrasekhar, J. G. Andrews, and A. Gatherer, "Femtocell networks: a survey," *IEEE Comm. Magazine*, vol. 46, no. 9, pp. 59–67, Sept. 2008.
- [2] M. S. Alouini and A. J. Goldsmith, "Area spectral efficiency of cellular mobile radio systems," *IEEE Trans. on Veh. Tech.*, vol. 48, no. 4, pp. 1047–1066, July 1999.
- [3] L. T. W. Ho and H. Claussen, "Effects of user-deployed, co-channel femtocells on the call drop probability in a residential scenario," in *Proc., IEEE International Symp. on Personal, Indoor and Mobile Radio Comm.*, Sept. 2007, pp. 1–5.

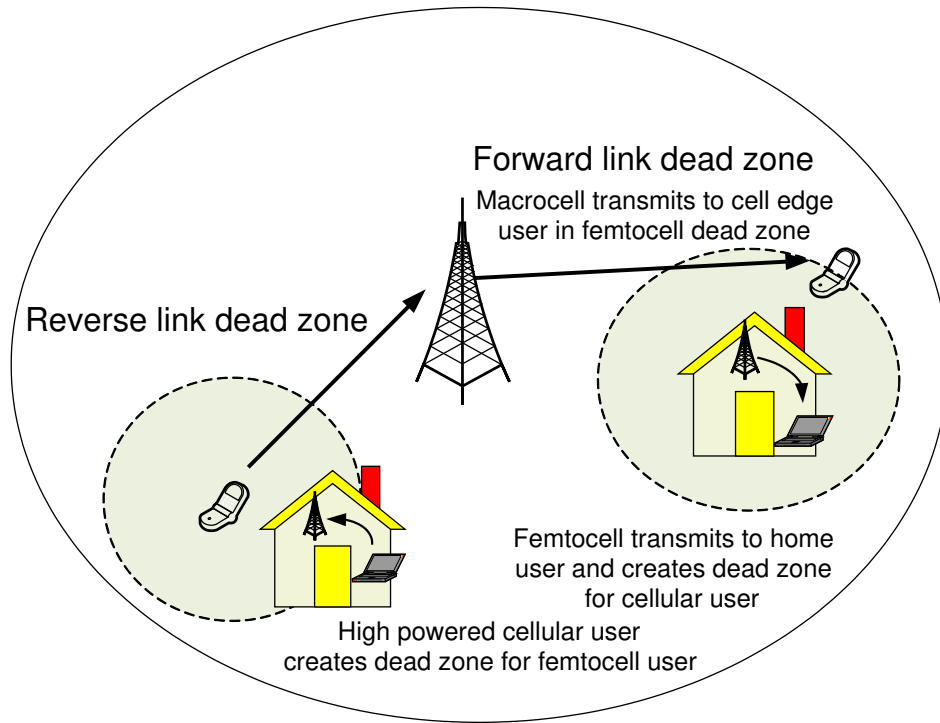


Fig. 1. Dead zones caused by cross-tier interference in a shared spectrum two-tier network.

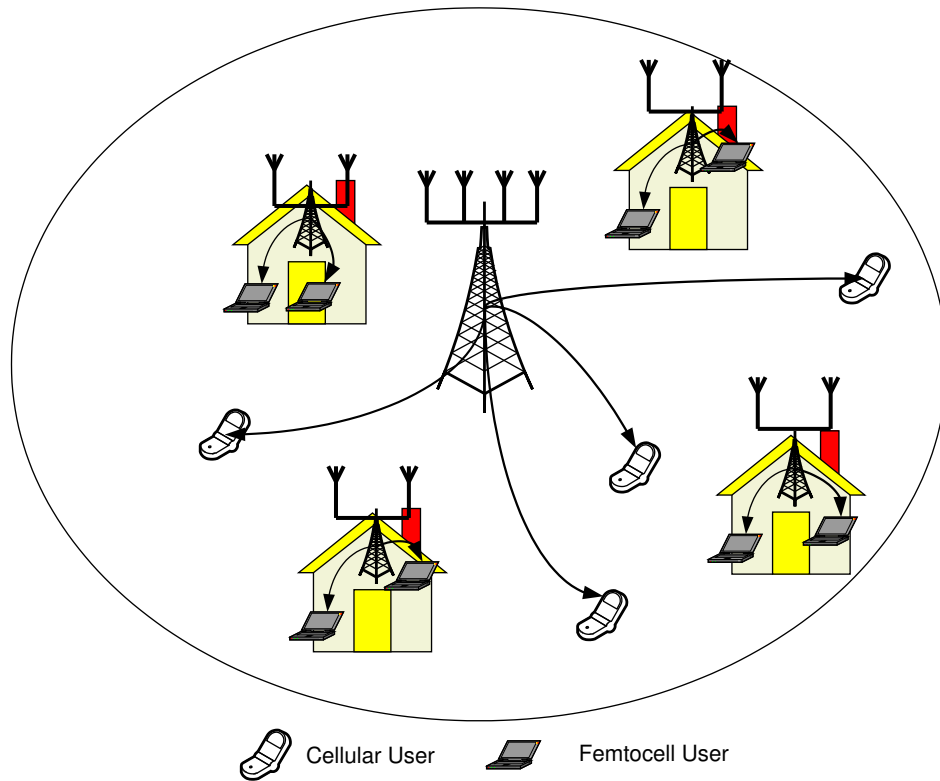


Fig. 2. Multiuser Multiple Antenna Transmission in a two-tier network.

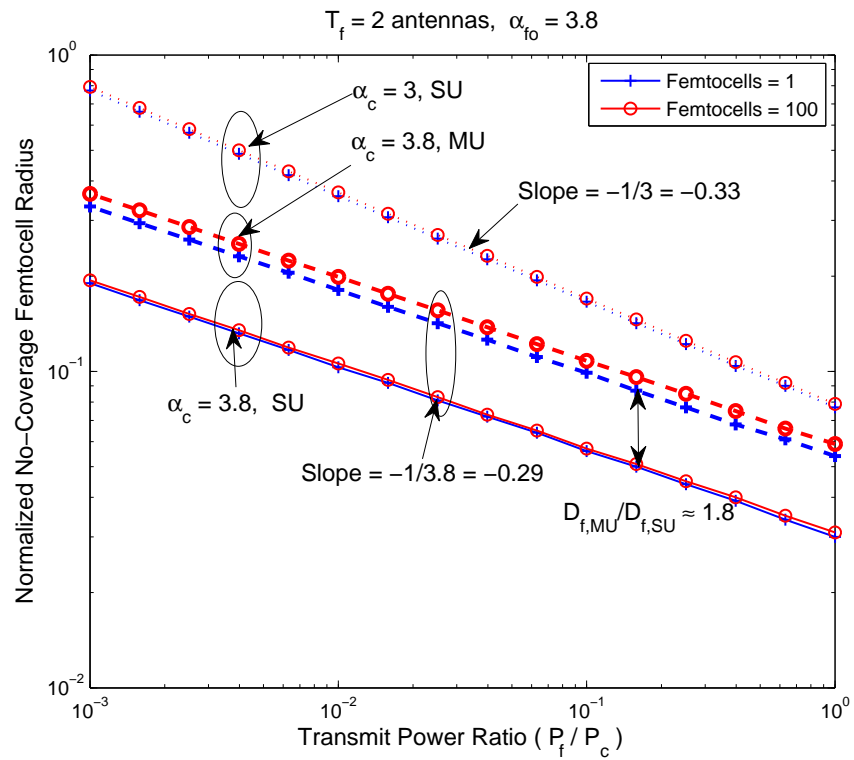


Fig. 3. No-coverage Femtocell Radius for different values of $\frac{P_f}{P_c}$.

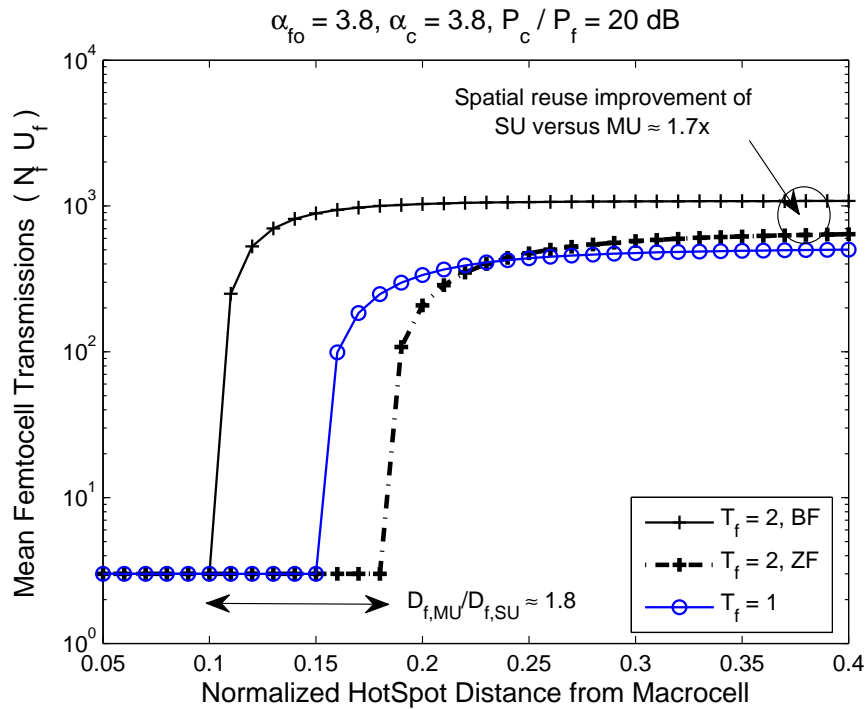


Fig. 4. Maximum number of simultaneous femtocell transmissions $N_f U_f$ for different number of antennas and single-user versus multiple-user transmission per femtocell.

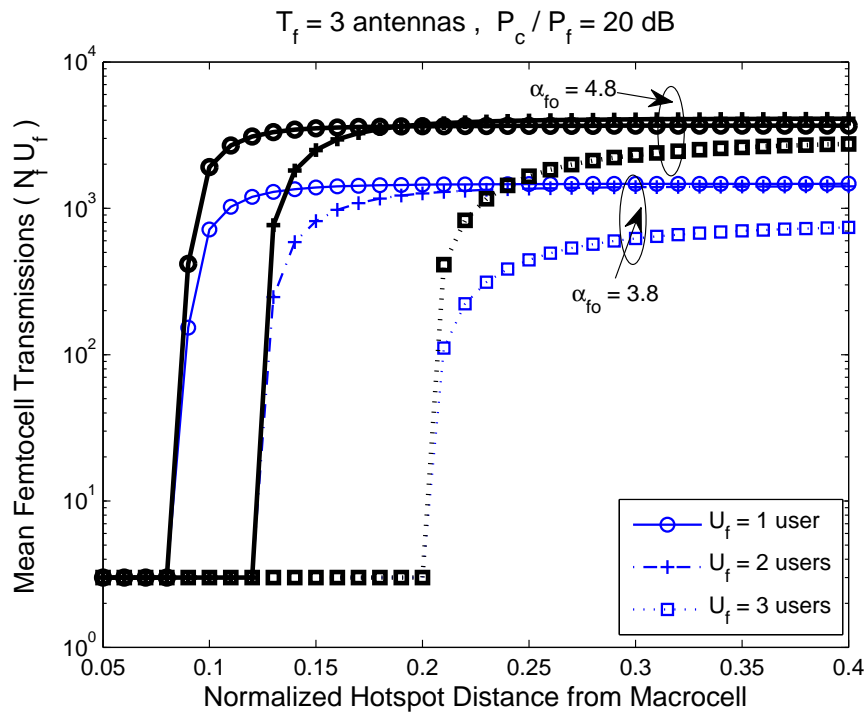


Fig. 5. Maximum number of simultaneous femtocell transmissions $N_f U_f$ for different values of α_{fo} .

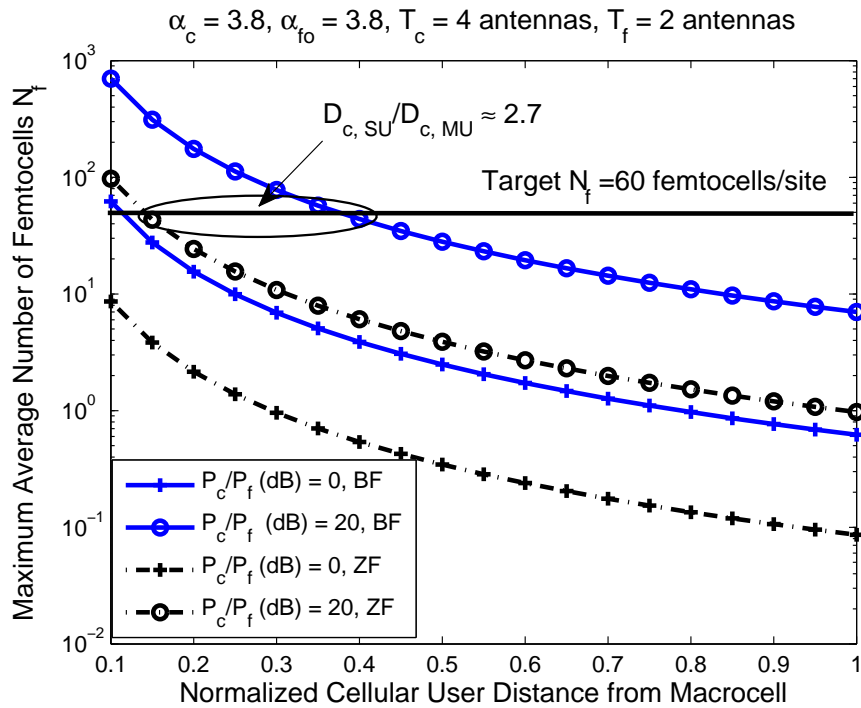


Fig. 6. Maximum number of simultaneous femtocell transmissions satisfying outage probability constraint ϵ for a cellular user at different distances from the macrocell.

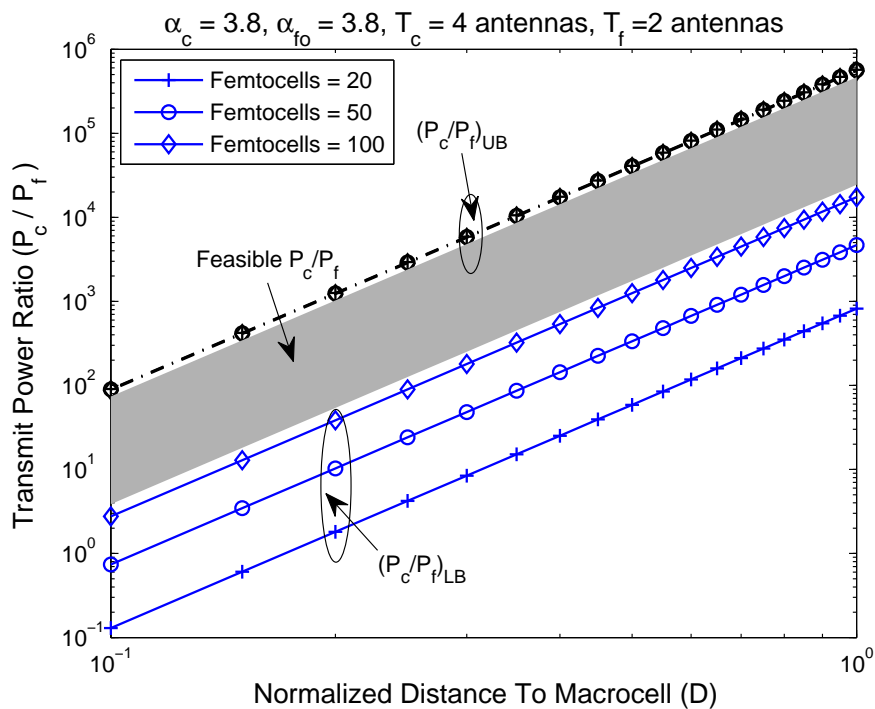


Fig. 7. Lower and Upper Bounds on P_c/P_f with SU transmission as a function of the distance D . Shaded region shows feasible P_c/P_f 's at location D , which satisfies the per-tier outage probability requirement for different average numbers of femtocells per cell-site.

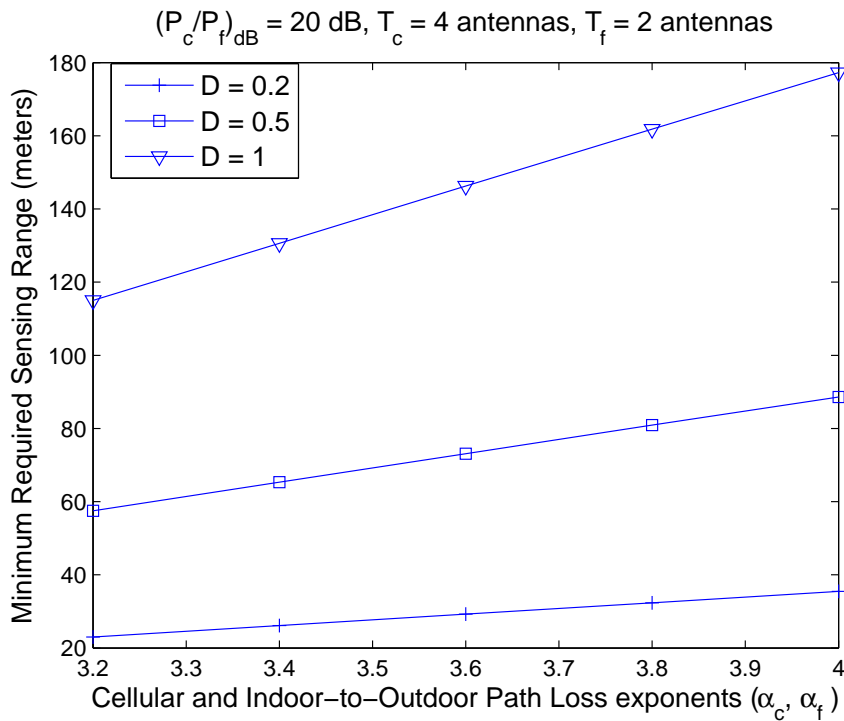


Fig. 8. Necessary Sensing Range (in meters) per femtocell (assuming SU transmission in each tier) as a function of the path loss exponents α_c, α_f and the normalized distance D of the cellular user.

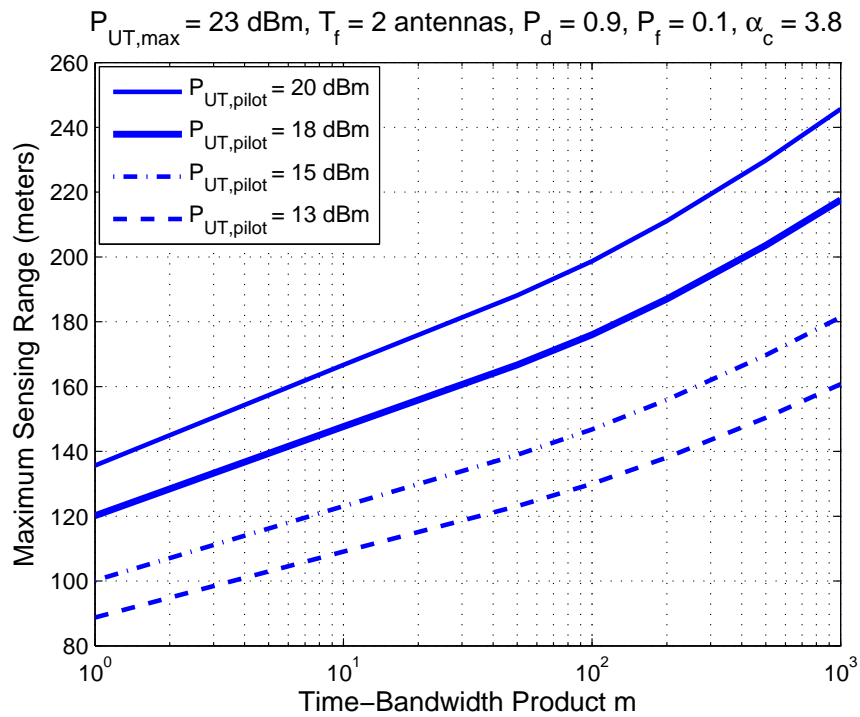


Fig. 9. Maximum Sensing Range (in meters) at each femtocell as a function of the sensing time-bandwidth product and uplink pilot transmission powers.

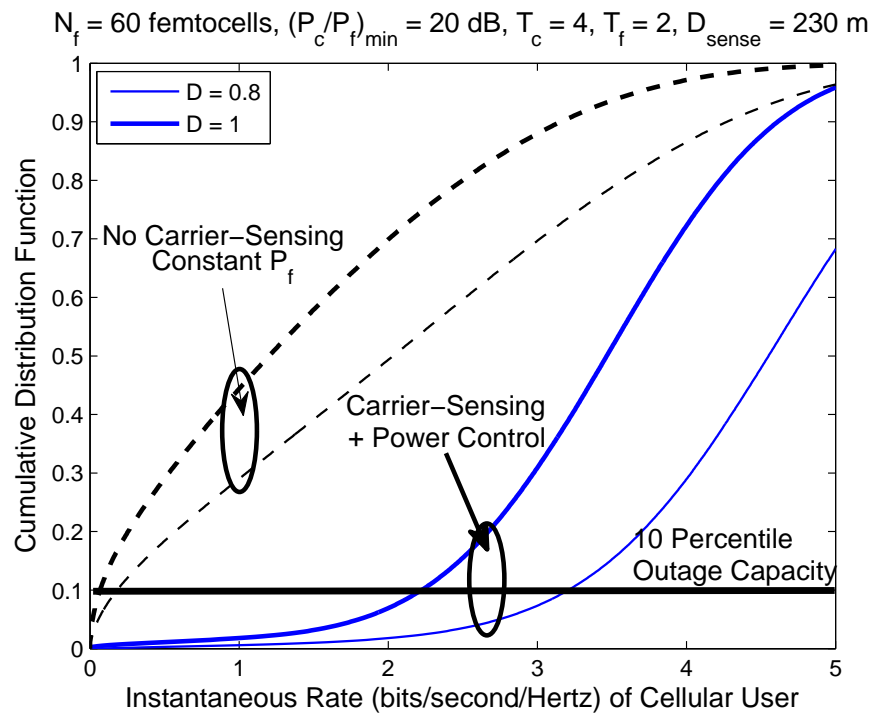


Fig. 10. Cumulative Distribution Function of the instantaneous cellular data rate (in b/s/Hz) with SU transmission in each tier. Performance of both randomized femtocell transmission and carrier-sensing femtocell transmission with power control are evaluated.

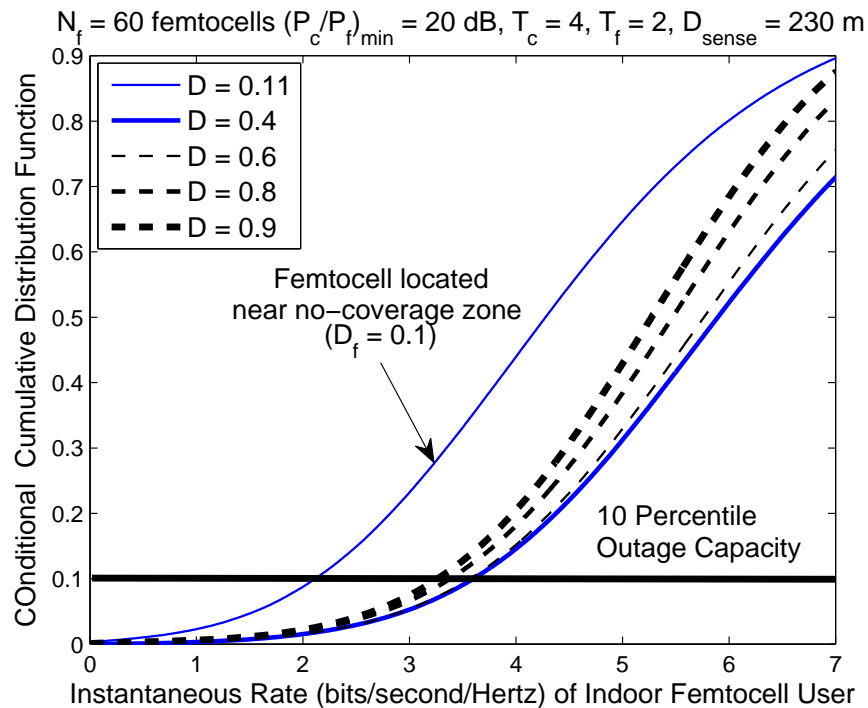


Fig. 11. Conditional Cumulative Distribution Function of the instantaneous Hotspot data rate (in b/s/Hz) (conditioned on a carrier-sensed cellular user at distance $D_{\text{sense}}/2$). Single-user transmission is employed in each tier.

- [4] A. Zemlianov and G. De Veciana, "Cooperation and decision-making in a wireless multi-provider setting," in *Proc., IEEE INFOCOM*, vol. 1, Mar. 2005, pp. 386–397.
- [5] A. Ganz, C. M. Krishna, D. Tang, and Z. J. Haas, "On optimal design of multitier wireless cellular systems," *IEEE Communications Magazine*, vol. 35, no. 2, pp. 88–93, Feb. 1997.
- [6] S. Kishore, L. J. Greenstein, H. V. Poor, and S. C. Schwartz, "Soft handoff and uplink capacity in a two-tier CDMA system," *IEEE Trans. on Wireless Comm.*, vol. 4, no. 4, pp. 1297–1301, July 2005.
- [7] B. Ahn, H. Yoon, and J. W. Cho, "A design of macro-micro CDMA cellular overlays in the existing big urban areas," *IEEE Journal on Sel. Areas in Comm.*, vol. 19, no. 10, pp. 2094–2104, Oct. 2001.
- [8] D. Niyato and E. Hossain, "Call admission control for QoS provisioning in 4G wireless networks: issues and approaches," *IEEE Network*, vol. 19, no. 5, pp. 5–11, Sept./Oct. 2005.
- [9] K. Yang, Y. Wu, and H.-H. Chen, "QoS-aware routing in emerging heterogeneous wireless networks," *IEEE Comm. Magazine*, vol. 45, no. 2, pp. 74–80, Feb. 2007.
- [10] T. E. Klein and S.-J. Han, "Assignment strategies for mobile data users in hierarchical overlay networks: performance of optimal and adaptive strategies," *IEEE Journal on Sel. Areas in Comm.*, vol. 22, no. 5, pp. 849–861, June 2004.
- [11] Z. Shen and S. Kishore, "Optimal multiple access to data access points in tiered CDMA systems," in *Proc., IEEE Veh. Tech. Conf.*, vol. 1, Sept. 2004, pp. 719–723.
- [12] H. Claussen, "Performance of macro- and co-channel femtocells in a hierarchical cell structure," in *Proc., IEEE International Symp. on Personal, Indoor and Mobile Radio Comm.*, Sept. 2007, pp. 1–5.
- [13] V. Chandrasekhar, J. G. Andrews, T. Muharemovic, Z. Shen, and A. Gatherer, "Power control in two-tier femtocell networks,"

- Submitted, IEEE Trans. on Wireless Comm.*, 2008, [Online] Available at <http://arxiv.org/abs/0810.3869>.
- [14] V. Chandrasekhar and J. G. Andrews, "Uplink capacity and interference avoidance in two-tier femtocell networks," *To appear, IEEE Trans. on Wireless Comm.*, 2009, [Online] Available at <http://arxiv.org/abs/cs.NI/0702132>.
- [15] K. Huang, V. Lau, and Y. Chen, "Spectrum sharing between cellular and mobile ad hoc networks: Transmission-capacity trade-off," *Submitted, IEEE Journal on Sel. Areas on Comm.*, 2008, [Online] Available at <http://arxiv.org/abs/0808.2181>.
- [16] A. M. Hunter, J. G. Andrews, and S. Weber, "Transmission capacity of ad hoc networks with spatial diversity," *IEEE Transactions on Wireless Communications*, vol. 7, pp. 5058–5071, Dec. 2008.
- [17] D. H. Kim, D. D. Lee, H. J. Kim, and K. C. Whang, "Capacity analysis of macro/microcellular CDMA with power ratio control and tilted antenna," *IEEE Transactions on Vehicular Technology*, vol. 49, no. 1, pp. 34–42, Jan. 2000.
- [18] Y.-C. Liang, Y. Zeng, E. C. Y. Peh, and A. T. Hoang, "Sensing-throughput tradeoff for cognitive radio networks," *IEEE Trans. on Wireless Comm.*, vol. 7, no. 4, pp. 1326–1337, Apr. 2008.
- [19] N. Hoven and A. Sahai, "Power scaling for cognitive radio," in *International Conf. on Wireless Networks, Communications and Mobile Computing*, vol. 1, June 2005, pp. 250–255.
- [20] K. Hamdi, W. Zhang, and K. Ben Letaief, "Power control in cognitive radio systems based on spectrum sensing side information," in *Proc., IEEE International Conf. on Comm.*, June 2007, pp. 5161–5165.
- [21] A. Ghasemi and E. Sousa, "Spectrum sensing in cognitive radio networks: the cooperation-processing tradeoff," *Wirel. Commun. Mob. Comput.*, vol. 7, no. 9, pp. 1049–1060, 2007.
- [22] L. Qian, X. Li, J. Attia, and Z. Gajic, "Power control for cognitive radio ad hoc networks," in *IEEE Workshop on Local & Metro. Area Netwks.*, June 2007, pp. 7–12.
- [23] J. Kingman, *Poisson Processes*. Oxford University Press, 1993.
- [24] M. Haenggi, J. G. Andrews, F. Baccelli, O. Dousse, and M. Franceschetti, "Stochastic geometry and random graphs for the analysis and design of wireless networks," *Submitted, IEEE Journal on Sel. Areas on Comm.*, 2009.
- [25] C. C. Chan and S. Hanly, "Calculating the outage probability in a CDMA network with Spatial Poisson traffic," *IEEE Trans. on Veh. Tech.*, vol. 50, no. 1, pp. 183–204, Jan. 2001.
- [26] F. Baccelli, B. Blaszczyszyn, and F. Tournois, "Spatial averages of coverage characteristics in large CDMA networks," *Wireless Networks*, vol. 8, no. 6, pp. 569–586, Nov. 2002.
- [27] F. Baccelli, B. Blaszczyszyn, and P. Muhlethaler, "An ALOHA protocol for multihop mobile wireless networks," *IEEE Trans. on Info. Theory*, vol. 52, no. 2, pp. 421–436, Feb. 2006.
- [28] "HNB and HNB-macro propagation models," in *3rd Generation Partnership Project, Tech. Rep. R4-071617*, Oct. 2007.
- [29] "Guidelines for evaluation of radio transmission technologies for IMT-2000," *ITU Recommendation M.1225*, 1997.
- [30] J. G. Andrews, A. Ghosh, and R. Muhamed, *Fundamentals of WiMAX*. Prentice-Hall, 2007.
- [31] A. K. Gupta and S. Nadarajan, *Handbook of Beta distribution and its applications*. Marcel Dekker Inc., 2004.
- [32] H. Urkowitz, "Energy detection of unknown deterministic signals," *Proceedings of the IEEE*, vol. 55, no. 4, pp. 523–531, Apr. 1967.
- [33] F. F. Digham, M. S. Alouini, and M. K. Simon, "On the energy detection of unknown signals over fading channels," in *Proc., IEEE International Conf. on Comm.*, vol. 5, May 2003, pp. 3575–3579.
- [34] J. H. Winters, J. Salz, and R. D. Gitlin, "The impact of antenna diversity on the capacity of wireless communication systems," *IEEE Trans. on Comm.*, vol. 42, pp. 1740–1751, 1994.
- [35] J. Lee and N. Jindal, "High SNR analysis for MIMO broadcast channels: Dirty paper coding versus linear precoding," *IEEE Trans. on Info. Theory*, vol. 53, no. 12, pp. 4787–4792, Dec. 2007.
- [36] Y. Akyildiz and B. D. Rao, "Statistical performance analysis of optimum combining with co-channel interferers and flat rayleigh fading," in *Proc., IEEE Global Telecomm. Conference*, vol. 6, San Antonio, TX, USA, 2001, pp. 3663–3667.
- [37] S. Lowen and M. Teich, "Power-law shot noise," *IEEE Trans. on Info. Theory*, vol. 36, no. 6, pp. 1302–1318, Nov. 1990.

- [38] E. Sousa and J. Silvester, "Optimum transmission ranges in a direct-sequence spread-spectrum multihop packet radio network," *IEEE Journal on Sel. Areas in Comm.*, vol. 8, no. 5, pp. 762–771, June 1990.
- [39] H. Gould, *Combinatorial Identities*. MorganTown Printing and Binding Co., 1972.